Pseudoscalar top-Higgs coupling: Exploration of CP-odd observables to resolve the sign ambiguity

Nicolas Mileo,[1,*] Ken Kiers,[2,†] Alejandro Szynkman,[1,‡] Daniel Crane ,[2,§] and Ethan Gegner[2,¶]

[1] *IFLP, CONICET – Dpto. de Física, Universidad Nacional de La Plata, C.C. 67, 1900 La Plata, Argentina*

[2] *Physics and Engineering Department, Taylor University, 236 West Reade Ave., Upland, IN 46989, USA*

(Dated: March 2, 2016)

Abstract

We present a collection of CP-odd observables for the process $pp \to t\,(\to b\ell^+\nu_\ell)\,\bar{t}\,\left(\to \bar{b}\ell^-\bar{\nu}_\ell\right) H$ that are linearly dependent on the scalar (κ_t) and pseudoscalar ($\tilde{\kappa}_t$) top-Higgs coupling and hence sensitive to the corresponding relative sign. The proposed observables are based on triple product (TP) structures that we extract from the expression of the differential cross section in terms of the spin vectors of the top and antitop quarks. In order to explore other possibilities, we progressively modify these TPs, first by combining them, and then by replacing the spin vectors by the lepton momenta or the t and $\bar{t}$ momenta by their visible parts. Assuming an integrated luminosity that is consistent with that envisioned for the HL-LHC, we find that the most promising observable can disentangle the hypotheses $\kappa_t = 1, \tilde{\kappa}_t = \pm 1$ by more than the $\sim 20\sigma$ statistical level. In the case of observables that do not need the reconstruction of the t and $\bar{t}$ momenta, the power of discrimination is up to the $\sim 16\sigma$ statistical level for the same number of events. We also show that the capability of the most promising observables for separating the CP-mixed hypotheses preveals even when a number of events plausible within the short term LHC is considered.

* mileo@fisica.unlp.edu.ar

† knkiers@taylor.edu

‡ szynkman@fisica.unlp.edu.ar

§ dkcrane@mtu.edu

¶ ethan_gegner@taylor.edu

I. INTRODUCTION

After the discovery of a new boson H by the ATLAS [1] and CMS [2] collaborations, it has become of crucial importance to determine its physical properties with the highest possible precision. The study of the new boson's couplings to fermions is of great relevance and will allow us to better understand this particle's CP-transformation properties, as well as the extent to which this particle is consistent with the Higgs boson predicted by the Standard Model (SM) of particle physics. It is of particular importance to test the coupling of the putative Higgs boson to the top quark. This coupling governs the main Higgs boson production mechanism (which proceeds via gluon fusion) and it contributes to the important Higgs boson decay mode to two photons. It is also involved in the scalar-field naturalness problem – giving rise to the leading dependence on the cut-off energy scale in the corrections to the Higgs mass – and it may play an important role in the mechanism for electroweak symmetry breaking.

Given that the main Higgs boson production process is dominated by a top quark loop and that the diphoton and digluon decay channels are also mediated by a top loop, these processes provide constraints on the scalar and pseudoscalar tH couplings, κ_t and $\tilde{\kappa}_t$ [3–6]. However, these constraints assume that there are no other sources contributing to the corresponding effective couplings; furthermore, in the case of the diphoton decay channel (which also involves a W boson loop), it is also assumed that the coupling of the Higgs boson to the W is standard. In this sense, the constraints derived from measurements of Higgs boson production and decay rates are indirect constraints. Electric dipole moments can also impose stringent indirect constraints on $\tilde{\kappa}_t$ by assuming that there are no new physics (NP) particles contributing to the loops of the relevant diagrams and in the case of the EDM of the electron that the electron-Higgs coupling is that predicted by the SM [3, 7]. In order to probe the tH coupling directly, processes with smaller cross sections need to be taken into account.

In contrast to the τH coupling, which can be studied through the decay $H \to \tau^+\tau^-$ [8], the tH coupling can only be tested directly via production processes, since the Higgs boson is kinematically forbidden from decaying to a $t\bar{t}$ pair. Two types of processes are of particular interest in this regard – the production of a Higgs boson in association with a $t\bar{t}$ pair and in association with a single top or antitop. The cross section for associated Higgs production with a single top (antitop) is smaller than that for production with a $t\bar{t}$ pair, and involves the interference between a diagram in which the Higgs is radiated from the top (antitop) leg and one with the Higgs emitted from the intermediate virtual W boson. Interestingly, this implies that the contraints on κ_t and $\tilde{\kappa}_t$ derived from tH and $\bar{t}H$ production are dependent on the assumption made regarding the coupling of the Higgs boson to the W gauge boson, κ_W. Nevertheless, it is important to note that the interference between the above mentioned diagrams can be exploited to determine the relative sign between κ_t and κ_W (see for example Ref. [9]). Associated Higgs production with a $t\bar{t}$ pair has been studied by several authors, and various observables sensitive to the couplings κ_t and $\tilde{\kappa}_t$ have been proposed. Examples of such observables (all of which are CP-even) are the cross section, invariant mass distributions, the transverse Higgs momentum distribution and the azimuthal angular separation between the t and $\bar{t}$, to name a few [10]. Also, an approach based on weighted moments and optimal observables has been developed in Ref. [11] to discriminate the hypothesis of a CP-even Higgs from that of a CP-mixed state within the context of an e^+e^- as well as a pp collider. Now, CP-even observables are not sensitive to the relative sign between the scalar and pseudoscalar couplings κ_t and $\tilde{\kappa}_t$. Such observables are quadratically dependent on these couplings and thus only provide an indirect measure of CP violation. In order to be sensitive to the relative sign

between κ_t and $\tilde{\kappa}_t$, CP-odd observables must be considered.

Since the top quark decays before it can hadronize, its spin information is passed on to the angular distributions of its decay products in such a way that these particles work as spin analyzers. As is well known, in the case of semileptonic top decay, the charged lepton is the most powerful in this regard. It is also known that the top quark and antiquark spins are highly correlated in $t\bar{t}$ production, a feature that is manifested in the double angular distributions of the decay products of the t and $\bar{t}$ systems [12]. In the case of $t\bar{t}H$ associated production, the $t\bar{t}$ spin correlations are also sensitive to the manner in which the top couples to the Higgs boson. In fact, observables that exploit the differences in the $t\bar{t}$ spin configurations were used in Ref. [13] to improve the discrimination of the $t\bar{t}H$ signal from the dominant irreducible background $t\bar{t}b\bar{b}$, which does not involve the Higgs boson.

In this paper, we define a set of observables that are linearly dependent on κ_t and $\tilde{\kappa}_t$ and are thus sensitive to the relative sign of these couplings. The proposed observables are based on a particular set of triple product (TP) structures that we extract naturally from the expression for the differential cross section for $pp \to t\ (\to b\ell^+\nu_\ell)\,\bar{t}\ \left(\to \bar{b}\ell^-\bar{\nu}_\ell\right)\ H$, making use of the fact that the t and $\bar{t}$ decay products contain spin information and are sensitive to the nature of the tH coupling, as noted above. By using spinor techniques we relate the top and antitop spin vectors to final state particle momenta and separate the production process from the decay. This allows to identify straightforwardly the contributions linearly sensitive to the couplings. Further, the TPs correlations in these contributions incorporate the t and $\bar{t}$ spin vectors. Starting with these TPs, we not only recover the observables given in [10, 14] but also propose additional possibilities that increase the sensitivity. In order to establish a hierarchy in the sensitivity of the TPs under analysis we investigate three different types of observables by using simulated events: asymmetries, mean values and angular distributions. We note that TP correlations have been used in [15] in the context of top-quark production and decay and in [16] in the framework of anomalous color dipole operators.

The remainder of this paper is organized as follows. In Sec. II we study the theoretical framework for the process $pp \to t\ (\to b\ell^+\nu_\ell)\,\bar{t}\ \left(\to \bar{b}\ell^-\bar{\nu}_\ell\right)\ H$ and derive a general expression for the differential cross section from which a first set of TP correlations is extracted. In Sec. III we probe the sensitivity of these TPs to the tH coupling by using various CP-odd observables. Subsequent sections are dedicated to explore another possibilities of CP-odd observables. In particular, observables based on TPs that incorporate the Higgs momentum are discussed in Sec. IV, whereas observables obtained without using the t and $\bar{t}$ momenta are studied in Sec. V. Finally, Sec. VI is devoted to the discussion on the experimental feasibility of the most promising observables encountered here. The main conclusions are summarized in Sec. VII.

II. THEORETICAL FRAMEWORK FOR $pp \to t(\to b\ell^+\nu_\ell)\,\bar{t}(\to \bar{b}\ell^-\bar{\nu}_\ell)\,H$

At the LHC $t\bar{t}H$ production proceeds via $q\bar{q}$ annihilation and gg fusion processes. The relevant leading-order Feynman diagrams are displayed in Fig. 1, where the first two rows show the $q\bar{q}$ and gg s-channel diagrams, and the last one depicts the gg t-channel diagrams. Three more gg-initiated diagrams are obtained by exchanging the gluon lines in the third row. We describe the tH coupling with the effective Lagrangian

$$\mathcal{L}_{t\bar{t}H} = -\frac{m_t}{v}(\kappa_t \bar{t}t + i\tilde{\kappa}_t \bar{t}\gamma_5 t)H, \tag{1}$$

where $v = 246$ GeV is the SM Higgs vacuum expectation value, and the coefficients κ_t and $\tilde{\kappa}_t$ parameterize the scalar and pseudoscalar interaction, respectively. The SM case is obtained for $\kappa_t = 1$ and $\tilde{\kappa}_t = 0$, while the values $\kappa_t = 0$ and $\tilde{\kappa}_t \neq 0$ parameterize a CP-odd Higgs boson.

Before turning to a discussion of CP-odd observables, it is useful to consider a few theoretical aspects of the process $pp \to t\,(\to b\ell^+\nu_\ell)\,\bar{t}\,\left(\to \bar{b}\ell^-\bar{\nu}_\ell\right)\,H$. In the following subsections we derive a "factorized" expression for the gluon fusion contribution to this process and then use this expression to isolate various mathematical quantities that will be useful as we construct CP-odd observables.

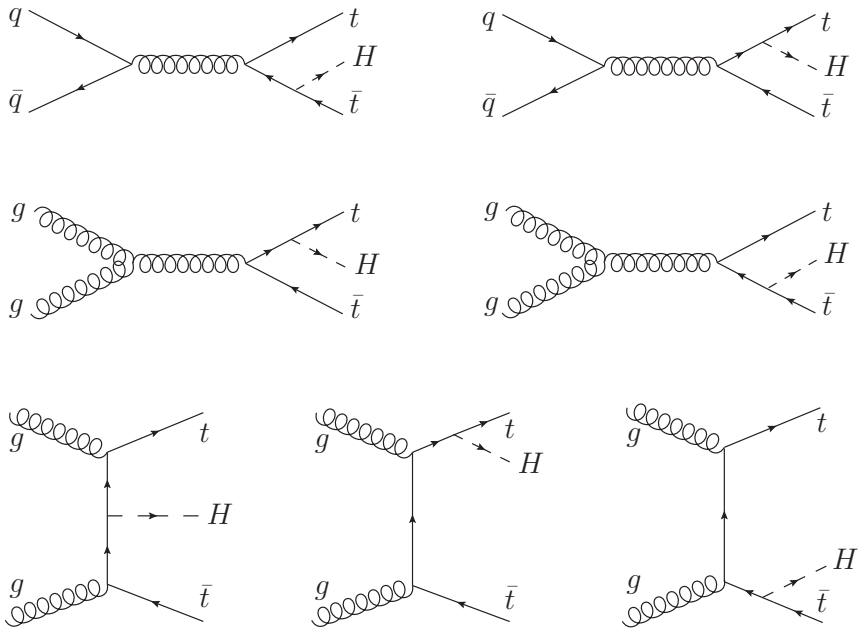

FIG. 1: Tree-level Feynman diagrams contributing to $t\bar{t}H$ production at the LHC. Three more diagrams are obtained by exchanging the gluon lines in the t-channel diagrams.

A. Factorized expression for the scattering cross section

In this subsection we focus on the gluon fusion **(KK: seems repetitive to say "gluon fusion" right away again... maybe can change this; maybe OK to leave it?)** contributions to $t\bar{t}H$ production, since these dominate over the the quark-antiquark annihilation contributions. Furthermore, we consider the case in which the top and antitop both decay semileptonically. As we shall show below, assuming the narrow width approximation for the top and antitop quarks, the unpolarized differential cross section for $gg \to t(\to b\ell^+\nu_\ell)\,\bar{t}(\to \bar{b}\ell^-\bar{\nu}_\ell)\,H$

may be written in the following "factorized" form,[1]

$$d\sigma = \sum_{\substack{b\ell^+\nu_l \\ \text{spins}}} \sum_{\substack{\bar{b}\ell^-\bar{\nu}_\ell \\ \text{spins}}} \left(\frac{2}{\Gamma_t}\right)^2 d\sigma(gg \to t(n_t)\bar{t}(n_{\bar{t}})H)\, d\Gamma(t \to b\ell^+\nu_\ell)\, d\Gamma(\bar{t} \to \bar{b}\ell^-\bar{\nu}_\ell), \tag{2}$$

where $d\sigma(gg \to t(n_t)\bar{t}(n_{\bar{t}})H)$ is the differential cross section for the production of a top and antitop quark, with spin vectors n_t and $n_{\bar{t}}$, respectively, along with a Higgs boson. Also, $d\Gamma(t \to b\ell^+\nu_\ell)$ and $d\Gamma(\bar{t} \to \bar{b}\ell^-\bar{\nu}_\ell)$ are the partial differential decay widths for an unpolarized top and anti-top quark. The four-vectors n_t and $n_{\bar{t}}$ are not arbitrary, but are given by particular combinations of the momenta of the $t, \bar{t}, \ell^+$ and ℓ^- [17],

$$n_t = -\frac{p_t}{m_t} + \frac{m_t}{(p_t \cdot p_{\ell^+})} p_{\ell^+} \tag{3}$$

$$n_{\bar{t}} = \frac{p_{\bar{t}}}{m_t} - \frac{m_t}{(p_{\bar{t}} \cdot p_{\ell^-})} p_{\ell^-}. \tag{4}$$

Expressions similar to Eq. (2) have been derived previously for the production of short-lived particles in e^-e^+ colliders [18] and for $t\bar{t}$ production both in e^-e^+ colliders [17] and pp colliders [19].

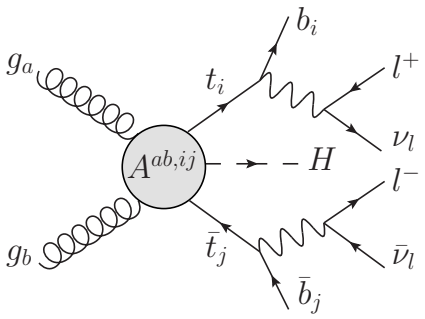

FIG. 2: Schematic representation of the process $g_a g_b \to t(\to b_i\ell^+\nu_\ell)\bar{t}(\to \bar{b}_j\ell^-\bar{\nu}_\ell)H$. The indices i, j denote the colour of the quarks while a, b are gluon indices.

To derive the above expressions, we begin by considering the schematic representation for the process $g_a g_b \to t(\to b_i\ell^+\nu_\ell)\,\bar{t}(\to \bar{b}_j\ell^-\bar{\nu}_\ell)\,H$ that is sketched in Fig. 2. Here a and b denote the initial-state gluons and i and j refer to the colours of the top and antitop quarks. The amplitude for this process may be written in the following compact form

$$\mathcal{M}^{ab,ij} = \bar{\psi}_t\, \mathcal{A}^{ab,ij}\, \psi_{\bar{t}}\,, \tag{5}$$

[1] The reader is referred to the discussion following Eq. (17) for some qualifying remarks regarding the "factorization" of this expression.

where the spinors $\bar{\psi}_t$ and $\psi_{\bar{t}}$ contain all of the information regarding the decay of the virtual top and anti-top, respectively, and where the quantity $A^{ab,ij}$ is given by

$$\mathcal{A}^{ab,ij} \equiv A^{ab,ij}_{\mu\nu}(\epsilon_{\lambda_a})^{\mu}(\epsilon_{\lambda_b})^{\nu} = \sum_{k=1}^{8} \mathcal{A}^{ab,ij}_k = \kappa_t \sum_{k=1}^{8} \mathcal{S}^{ab,ij}_k + i\tilde{\kappa}_t \sum_{k=1}^{8} \mathcal{P}^{ab,ij}_k. \tag{6}$$

The sum over k in the above expression corresponds to the eight gluon-initiated diagrams indicated in Fig. 1; also, ϵ_{λ_a} and ϵ_{λ_b} are the polarization vectors corresponding to g_a and g_b, respectively. In the last equality in Eq. (6) we have explicitly separated the amplitude into two sums, with one sum corresponding to the scalar contributions and the other to the pseudoscalar ones. Taking all of the final-state particles to be massless, we can use the spinor techniques developed in [20] to write $\bar{\psi}_t$ and $\psi_{\bar{t}}$ as follows[2]

$$\bar{\psi}_t = -g^2\, \mathbb{P}_t(t)\, \mathbb{P}_W(t-b)\, \langle b-|\nu_\ell+\rangle \langle \ell^+ + |(\not{t} + m_t) \tag{7}$$

$$\psi_{\bar{t}} = g^2\, \mathbb{P}_t(\bar{t})\, \mathbb{P}_W(\bar{t}-\bar{b})\, \langle \bar{\nu}_\ell + |\bar{b}-\rangle (\not{\bar{t}} - m_t)|\ell^- +\rangle, \tag{8}$$

where $|i+(-)\rangle \equiv (1/2)(1 \pm \gamma^5)\,\psi_i$ represents a right-handed (left-handed) chiral spinor for final-state particle i and $\langle i+(-)|$ represents the corresponding adjoint spinor. Also, $\mathbb{P}_t(q) = (q^2 - m_t^2 + i m_t \Gamma_t)^{-1}$ and $\mathbb{P}_W(q) = (q^2 - m_W^2 + i m_W \Gamma_W)^{-1}$, and we have denoted the momenta of the various particles by the symbols that refer to the names of those particles [21].

Using the expressions defined above for $\bar{\psi}_t$ and $\psi_{\bar{t}}$, we can write the amplitude $\mathcal{M}^{ab,ij}$ in a form that is (in a sense) factorized. As a first step, we insert Eqs. (7) and (8) into Eq. (5), yielding

$$\mathcal{M}^{ab,ij} = -g^4\, \mathbb{P}_t(t)\, \mathbb{P}_t(\bar{t})\, \mathbb{P}_W(t-b)\, \mathbb{P}_W(\bar{t}-\bar{b})\, \langle b-|\nu_\ell+\rangle \langle \bar{\nu}_\ell + |\bar{b}-\rangle \sqrt{2(t\cdot\ell^+)}\sqrt{2(\bar{t}\cdot\ell^-)}\, [\bar{\phi}_t \mathcal{A}^{ab,ij} \phi_{\bar{t}}], \tag{9}$$

where the spinors ϕ_t and $\phi_{\bar{t}}$ are defined as

$$\phi_t = \frac{(\not{t} + m_t)}{\sqrt{2(t\cdot\ell^+)}} |\ell^+ +\rangle \tag{10}$$

$$\phi_{\bar{t}} = \frac{(\not{\bar{t}} - m_t)}{\sqrt{2(\bar{t}\cdot\ell^-)}} |\ell^- +\rangle\,. \tag{11}$$

Note that in writing down the above expressions we have adopted the narrow-width approximation for the top and antitop quarks and for the $W^\pm$ gauge bosons.[3] Working out the projection operators $\phi_t\,\bar{\phi}_t$ and $\phi_{\bar{t}}\,\bar{\phi}_{\bar{t}}$, we have

$$\phi_t\,\bar{\phi}_t = \frac{1}{2}(1 + \not{\eta}_t \gamma^5)(\not{t} + m_t) \tag{12}$$

and

$$\phi_{\bar{t}}\,\bar{\phi}_{\bar{t}} = \frac{1}{2}(1 + \not{\eta}_{\bar{t}} \gamma^5)(\not{\bar{t}} - m_t), \tag{13}$$

---

[2] These spinor techniques can also be used for massive final-state particles. Given the energy scale involved in the process in question, however, the assumption of massless final-state particles is sensible and greatly simplifies the derivation of Eq. (2).

[3] Since Eq. (9) contains the top quark propagator term $\mathbb{P}_t(t)$, for example, $|\mathcal{M}^{ab,ij}|^2$ contains the factor $((t^2 - m_t^2)^2 + m_t^2\Gamma_t^2)^{-1}$, which is replaced by $(\pi/m_t\Gamma_t)\delta(t^2 - m_t^2)$ in the narrow-width approximation. Thus, except for the propagator terms $\mathbb{P}_t(t)$ and $\mathbb{P}_t(\bar{t})$, we take the four-vector t appearing in Eqs. (9)-(11) to be on shell, satisfying $t^2 = m_t^2$.

with n_t and $n_{\bar{t}}$ being the four-vectors defined in Eqs. (3) and (4). Thus, ϕ_t and $\phi_{\bar{t}}$ may be regarded as describing a top quark with spin vector n_t and an antitop quark with spin vector $n_{\bar{t}}$, respectively.

As a final step toward factorizing the amplitude $\mathcal{M}^{ab,ij}$, we note that the amplitude for a top quark with spin vector n_t to decay into $b\ell^+\nu_\ell$ is given by

$$\mathcal{M}(t(n_t) \to b\ell^+\nu_\ell) = ig^2\mathbb{P}_W(t-b)\langle b - |\nu_\ell +\rangle\sqrt{2(t\cdot\ell^+)}\,, \tag{14}$$

and likewise,

$$\mathcal{M}(\bar{t}(n_{\bar{t}}) \to \bar{b}\ell^-\bar{\nu}_\ell) = ig^2\mathbb{P}_W(\bar{t}-\bar{b})\langle\bar{\nu}_\ell + |\bar{b}-\rangle\sqrt{2(\bar{t}\cdot\ell^-)}. \tag{15}$$

Furthermore, the term inside the square brackets in Eq. (9) is the amplitude for producing a top quark with spin vector n_t, along with an anti-top with spin vector $n_{\bar{t}}$ and a Higgs boson,

$$\mathcal{M}(g_a g_b \to t^i(n_t)\bar{t}^j(n_{\bar{t}})H) = \bar{\phi}_t\mathcal{A}^{ab,ij}\phi_{\bar{t}}. \tag{16}$$

Combining Eqs. (14)-(16), we can write Eq. (9) in a form that appears to be factorized,

$$\mathcal{M}^{ab,ij} = \mathbb{P}_t(t)\mathbb{P}_t(\bar{t})\,\mathcal{M}(t(n_t)\to b\ell^+\nu_\ell)\,\mathcal{M}(\bar{t}(n_{\bar{t}})\to\bar{b}\ell^-\bar{\nu}_\ell)\,\mathcal{M}(g_ag_b\to t^i(n_t)\bar{t}^j(n_{\bar{t}})H)\,. \tag{17}$$

It is important to note that, even though the above expression has the appearance of being factorized into production and decay parts, this apparent factorization is a bit misleading. In particular, the amplitude for $t\bar{t}H$ production contains the top and antitop quark spin four-vectors n_t and $n_{\bar{t}}$, which depend on final-state kinematical quantities [see Eqs. (3) and (4)]. With this qualification in mind, we may now use the amplitude in Eq. (17) to determine the corresponding scattering cross section. After some manipulation of the phase space variables to take advantage of the presence of the propagator terms, $\mathbb{P}_t(t)$ and $\mathbb{P}_t(\bar{t})$, we arrive at the expression in Eq. (2).[4] This expression also has the appearance of being factorized, but qualifying remarks, similar to those above, apply.

B. Origin of triple product terms

The expression derived above for the scattering cross section [see Eq. (2), as well as Eq. (17)] provides significant insight into how one might analyze $pp \to t\,(\to b\ell^+\nu_\ell)\,\bar{t}\,\left(\to \bar{b}\ell^-\bar{\nu}_\ell\right)\,H$ in order to determine the nature of the top-Higgs coupling. In particular, let us focus on the production amplitude, $\mathcal{M}(g_ag_b\to t^i(n_t)\bar{t}^j(n_{\bar{t}})H))$, which forms part of the overall amplitude in Eq. (17). The absolute value squared of the production amplitude is used to determine $d\sigma(gg\to t(n_t)\bar{t}(n_{\bar{t}})H)$, which in turn forms part of the expression for the "factorized" cross section in Eq. (2). Summing over colour and gluon indices we have

$$\sum_{\substack{a,b\\i,j}}|\mathcal{M}(g_ag_b\to t^i(n_t)\bar{t}^j(n_{\bar{t}})H)|^2 = \sum_{\substack{a,b\\i,j}}\left|\sum_{k=1}^{8}C_k^{ab,ij}\,\bar{\phi}_t(\kappa_t\mathcal{S}_k + i\tilde{\kappa}_t\mathcal{P}_k)\phi_{\bar{t}}\right|^2, \tag{18}$$

[4] The reader may note that in the differential widths of $t\to b\ell^+\nu_\ell$ and $\bar{t}\to\bar{b}\ell^-\bar{\nu}_\ell$ appearing in Eq. (2), the spin states of the top an antitop have been averaged. Interestingly, under the assumption of massless final-state particles, the amplitudes $\mathcal{M}(t(-n_t)\to b\ell^+\nu_\ell)$ and $\mathcal{M}(\bar{t}(-n_{\bar{t}})\to\bar{b}\ell^-\bar{\nu}_\ell)$ vanish.

where we have separated the colour structure of each diagram by defining $\mathcal{S}_k^{ab,ij} = C_k^{ab,ij}\mathcal{S}_k$ and $\mathcal{P}_k^{ab,ij} = C_k^{ab,ij}\mathcal{P}_k$ [see Eqs. (6) and (16)]. Also, the factors $g_s^2 m_t/v$ and $-ig_s^2 m_t/v$ arising from the vertices of the t- and s-channel diagrams respectively have been included in the definition of $C_k^{ab,ij}$ for convenience. The terms linear in κ_t and $\tilde{\kappa}_t$ can be written as

$$\mathcal{O}(\kappa_t\tilde{\kappa}_t) \to \frac{1}{2}\kappa_t\tilde{\kappa}_t \sum_{k,r} \mathbb{C}_{kr}\mathrm{Im}\left\{\mathrm{Tr}\left[(1+\not{n}_t\gamma^5)(\not{t}+m_t)\mathcal{S}_k(1+\not{n}_{\bar{t}}\gamma^5)(\not{\bar{t}}-m_t)\tilde{\mathcal{P}}_r\right]\right\}, \tag{19}$$

where the factor $\mathbb{C}_{kr} = \sum_{ab,ij} C_k^{ab,ij} C_r^{ab,ij*}$ is real and where $\tilde{\mathcal{P}}_r = \gamma^0\mathcal{P}_r^\dagger\gamma^0$. The only terms that yield non-zero contributions in the above sum are those with an odd number of γ^5 matrices; these lead to triple-product (TP) structures of the form $\epsilon_{\alpha\beta\gamma\delta}\, p_a^\alpha p_b^\beta p_c^\gamma p_d^\delta$, where p_a-p_d represent various four momenta associated with the process. In contrast, it can be seen from Eq. (18) that the terms proportional to κ_t^2 and $\tilde{\kappa}_t^2$ descend from traces containing an even number of γ^5 matrices and can be written in terms of scalar products of the available momenta.

With the above considerations in mind, it is useful to write a general expression for the differential cross section $d\sigma(gg \to t(n_t)\bar{t}(n_{\bar{t}})H)$ in terms of the momenta $q = (q_1 - q_2)/2$, $Q = (q_1 + q_2)/2$, t, $\bar{t}$, n_t and $n_{\bar{t}}$, where $q_{1,2}$ denote the momenta of the initial-state gluons. Note that with this choice, $q \cdot Q = 0$ and $Q^2 = -q^2 = M_{t\bar{t}H}^2/4$, where $M_{t\bar{t}H}$ is the invariant mass of the $t\bar{t}H$ system. Fifteen TPs can be constructed from these six four-vectors,[5] so that

$$d\sigma(gg \to t(n_t)\bar{t}(n_{\bar{t}})H) = \kappa_t^2\, f_1(p_i\cdot p_j) + \tilde{\kappa}_t^2\, f_2(p_i\cdot p_j) + \kappa_t\tilde{\kappa}_t \sum_{l=1}^{15} g_l(p_i\cdot p_j)\,\epsilon_l, \tag{20}$$

where $\epsilon_l = \epsilon_{\alpha\beta\gamma\delta}\, p_a^\alpha p_b^\beta p_c^\gamma p_d^\delta$ denotes the lth TP (we adopt the convention $\epsilon_{0123} = +1$) and where p_i and p_j refer to any of the six momenta. The functions $f_{1,2}$ and g_k depend only on the possible scalar products and are therefore even under a parity transformation (P). However, the terms linear in $\kappa_t\tilde{\kappa}_t$ are P-odd due to the presence of the P-odd TPs. Hence, only the functions $f_{1,2}$ will contribute to the total cross-section, whereas the TP terms will be sensitive to the sign of the anomalous coupling $\tilde{\kappa}_t$. Of the fifteen TPs mentioned above, we will focus on those that contain both of the spin vectors n_t and $n_{\bar{t}}$, but do not include q. The decision not to consider q-dependent TPs is motivated by the fact that q cannot be expressed in terms of the momenta of final state particles (as Q can, by virtue of energy-momentum conservation). The decision to focus on TPs that contain both n_t and $n_{\bar{t}}$ is rooted in the fact that the spins of pair-produced top and antitop quarks are highly correlated at hadron colliders (even though the quarks themselves are unpolarized). Observables that combine the decay products of the t and $\bar{t}$ will be sensitive to this spin correlation [23]. A similar behaviour is expected in $t\bar{t}H$ production, where it can be shown that single-spin asymmetries vanish [13, 14]. Hence, in order to construct observables sensitive to the structure of the tH coupling, we will restrict our attention to those TPs that include information on the decay products of both the top and anti-top quarks. Only five of the fifteen TPs in Eq. (20) do not involve the four vector q and, among these, only three include both n_t and $n_{\bar{t}}$. Thus, we will restrict our attention to the following TPs

$$\epsilon_1 \equiv \epsilon(t, \bar{t}, n_t, n_{\bar{t}}), \tag{21}$$

$$\epsilon_2 \equiv \epsilon(Q, \bar{t}, n_t, n_{\bar{t}}), \tag{22}$$

[5] We note that these fifteen TPs are not linearly independent (see the epsilon relations discussed in Ref. [22]).

$$\epsilon_3 \equiv \epsilon(Q, t, n_t, n_{\bar{t}}). \tag{23}$$

Before turning to a consideration of various CP-odd observables, we remark that even though all of the above discussion took place within the context of gg-initiated production, similar conclusions are obtained for $q\bar{q}$-initiated production. In particular, the definitions of the spin vectors in Eqs. (3)-(4) and the general form of $d\sigma$ introduced in Eq. (20) are valid in both cases.

III. CP-ODD OBSERVABLES

In this section we present three types of observables based on the TPs discussed in Sec. II, namely, asymmetries, angular distributions and mean values. These observables are sensitive not only to the magnitude of the pseudoscalar coupling $\tilde{\kappa}_t$, but also to its sign. In order to test the various observables, we have used `MadGraph5_aMC@NLO` [24] to simulate the process $pp \to t\,(\to b\ell^+\nu_\ell)\,\bar{t}\,\left(\to \bar{b}\ell^-\bar{\nu}_\ell\right)\,H$ at parton level for different values of the couplings κ_t and $\tilde{\kappa}_t$. In all cases we have generated 10^5 events and have assumed a center-of-mass energy of 14 TeV.[6] We have also imposed the following set of cuts: p_T of leptons $> 10\,\text{GeV}$, $|\eta|$ of leptons < 2.5, $|\eta|$ of b jets < 2.5 and $\Delta R_{\ell\ell} > 0.4$. Note that we have used this somewhat large number of events (10^5) in order to determine clearly the extent to which the proposed observables are sensitive to the NP coupling. Section VI contains an analysis of the experimental feasibility of the more promising observables.

Before continuing on to our analysis, let us make a few comments regarding the values that we choose for κ_t and $\tilde{\kappa}_t$. First of all, we note that if the pseudoscalar coupling $\tilde{\kappa}_t$ is the only source of physics beyond the SM, then indirect contraints (based on the signal strength of $gg \to H \to \gamma\gamma$) disfavour $\kappa_t < 0$ but do not resolve the degeneracy in the sign of $\tilde{\kappa}_t$ [10]. On the other hand, if one assumes that the tensor structure of the Higgs interactions are the same as those of the SM and if one parameterizes these interactions via one universal Higgs coupling to vector bosons, κ_V, and one universal Higgs coupling to fermions, κ_f, then the measured signal strengths provided by the ATLAS and CMS collaborations are compatible with the values predicted by the SM, (namely, $\kappa_f = 1$ and $\kappa_V = 1$). With these facts in mind, we will, for the most part, set the value of the scalar coupling to its SM value ($\kappa_t = 1$) and will allow the pseudoscalar coupling to take on various values (including both possible signs). In particular, we analyze the cases $\tilde{\kappa}_t = 0, \pm 0.25, \pm 0.5, \pm 0.75, \pm 1$. In addition, we also provide some analysis regarding the pure CP-odd case ($\kappa_t = 0, \tilde{\kappa}_t = 1$).

A. Asymmetry

The first type of CP-odd observable that we will consider is an asymmetry that compares the number of events for which a given TP is positive to that for which it is negative. Normalizing to the total number of events, we define

$$\mathcal{A}(\epsilon) = \frac{N(\epsilon > 0) - N(\epsilon < 0)}{N(\epsilon > 0) + N(\epsilon < 0)}. \tag{24}$$

[6] Note that, since we generate the same number of events in each case, the corresponding integrated luminosities are different, since the cross section depends on the value of $\tilde{\kappa}_t$.

By construction, $\mathcal{A} \in [-1, +1]$. Based on the general expression given in Eq. (20), we expect the following functional form for the asymmetry,

$$\mathcal{A}(\epsilon) = \frac{A\kappa_t\tilde{\kappa}_t}{B\kappa_t^2 + C\tilde{\kappa}_t^2}, \tag{25}$$

which for $\kappa_t = 1$ can be parameterized as

$$\mathcal{A}(\epsilon) = \frac{a\tilde{\kappa}_t}{1 + b\tilde{\kappa}_t^2}, \tag{26}$$

where the parameter $a \equiv A/B$ determines the sensitivity to the pseudoscalar coupling, whereas $b \equiv C/B$ quantifies the deviation from linear behaviour.

Table I shows numerical results for the asymmetries associated with three different TPs, ϵ_1, ϵ_2 and ϵ_3, taking $\kappa_t = 1$ and $\tilde{\kappa}_t = 0, \pm 1$. The asymmetry $\mathcal{A}$ is shown in each case, along with $\mathcal{A}/\sigma_{\mathcal{A}}$, where $\sigma_{\mathcal{A}}$ is the corresponding statistical uncertainty. As is evident from the table, the asymmetries in question provide a clear separation between the SM and the CP-mixed cases, with typical deviations being of order 10σ. Furthermore, the asymmetries for the SM case are each statistically consistent with zero, as one would expect. The three asymmetries also allow one to determine the sign of $\tilde{\kappa}_t$, with deviations between the $\tilde{\kappa}_t = \pm 1$ cases typically being of order 20σ. **(We couldn't figure out how to clarify this. If you find a way go ahead. . . .)** The sensitivity of the asymmetry is quite similar for the three TPs, as can be seen by including other values of $\tilde{\kappa}_t$ and using the expression in Eq. (26) as a fitting function (see Fig. 3). Performing such a fit, we obtain $(a = -0.057 \pm 0.006, b = 0.5 \pm 0.2), (a = -0.056 \pm 0.006, b = 0.5 \pm 0.2)$ and $(a = 0.058 \pm 0.006, b = 0.6 \pm 0.2)$ for ϵ_1, ϵ_2 and ϵ_3, respectively.

The results shown in Table I and Fig. 3 all assume a pp initial state, which is actually a combination of events coming from gg and $q\bar{q}$ initial states. While this combination of initial states is the appropriate scenario to consider, it is interesting to consider the relative contributions to the asymmetry coming from the gg and $q\bar{q}$ initial states. Figure 4 shows three curves for the "ϵ_1" case, one for gg-initiated events, one for $q\bar{q}$-initiated events, and one for the usual combination of these events (the "pp" initial state). Interestingly, we see from Fig. 4 that the asymmetry for this TP is enhanced for gg-initiated production, while it is reduced and of opposite sign for the $q\bar{q}$-initiated events. The asymmetry for the pp case is evidently dominated by the gg contribution, but is somewhat smaller in magnitude due to the $q\bar{q}$ contribution.

TABLE I: Asymmetries for three different scenarios, obtained by using 10^5 simulated events for the TPs $\epsilon_1 = \epsilon(t, \bar{t}, n_t, n_{\bar{t}}), \epsilon_2 = \epsilon(Q, \bar{t}, n_t, n_{\bar{t}})$ and $\epsilon_3 = \epsilon(Q, t, n_t, n_{\bar{t}})$. The three scenarios correspond to the SM ($\kappa_t = 1$ and $\tilde{\kappa}_t = \pm 0$) and two CP-mixed cases (defined by $\kappa_t = 1$ and $\tilde{\kappa}_t = \pm 1$).

κ_t	$\tilde{\kappa}_t$	$\mathcal{A}(\epsilon_1)$	$\mathcal{A}(\epsilon_1)/\sigma_{\mathcal{A}}$	$\mathcal{A}(\epsilon_2)$	$\mathcal{A}(\epsilon_2)/\sigma_{\mathcal{A}}$	$\mathcal{A}(\epsilon_3)$	$\mathcal{A}(\epsilon_3)/\sigma_{\mathcal{A}}$
1	-1	0.0315	10.0	0.0332	10.5	-0.0307	-9.7
1	0	-0.0021	-0.7	0.0009	0.3	-0.0011	-0.3
1	1	-0.0379	-12.0	-0.0411	-13.0	0.0378	12.0

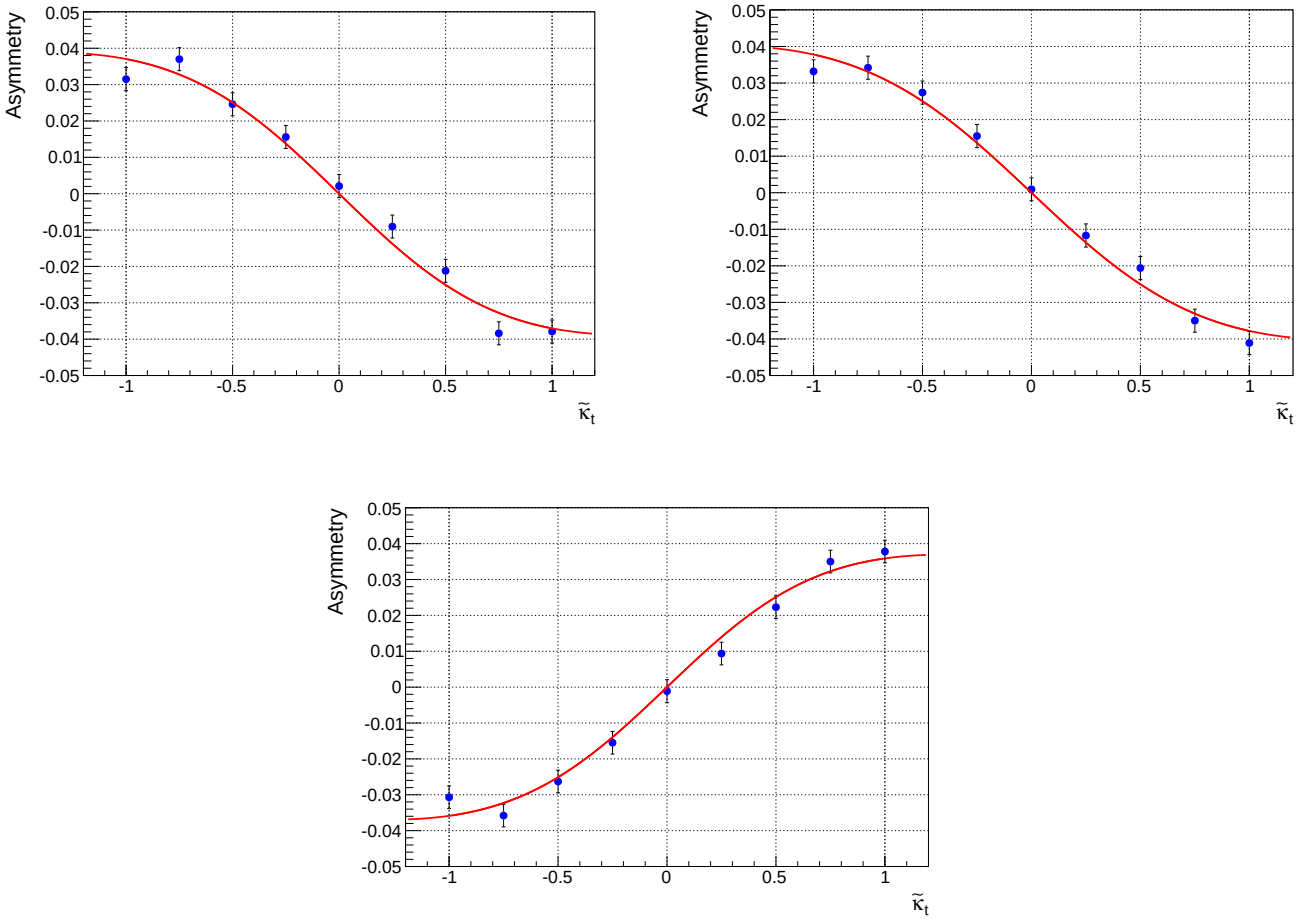

FIG. 3: Asymmetries for the TPs $\epsilon_1 = \epsilon(t, \bar{t}, n_t, n_{\bar{t}})$ (top-left), $\epsilon_2 = \epsilon(Q, \bar{t}, n_t, n_{\bar{t}})$ (top-right) and $\epsilon_3 = \epsilon(Q, t, n_t, n_{\bar{t}})$ (bottom). The points represent the values for $\tilde{\kappa}_t = 0, \pm 0.25, \pm 0.5, \pm 0.75, \pm 1$ and the red solid line is the fitting curve.

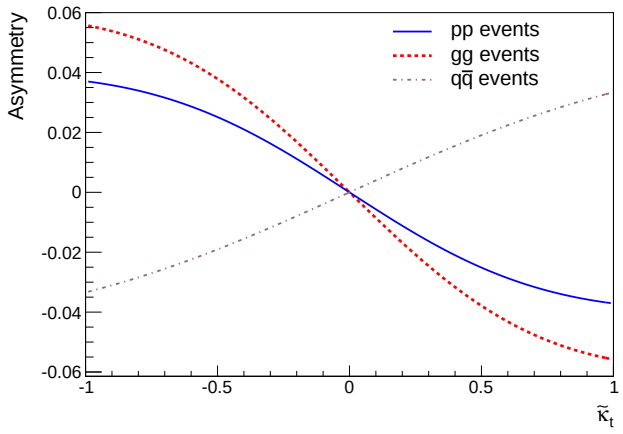

FIG. 4: Asymmetry for the TP $\epsilon_1 = \epsilon(t, \bar{t}, n_t, n_{\bar{t}})$. The dashed line (red) corresponds to gg-initiated production, the dot-dashed line (grey) to $q\bar{q}$-initiated production and the solid line (blue) to pp production.

We have also tested various linear combinations of the TPs $\epsilon_{1,2,3}$ and have found that the asymmetry is enhanced for the following combination:

$$\epsilon_4 = \epsilon_3 - \epsilon_2 = \epsilon(Q, t - \bar{t}, n_t, n_{\bar{t}}). \tag{27}$$

Note that in the Q rest frame, $\epsilon_4 = Q^0(\vec{t} - \vec{\bar{t}}) \cdot (\vec{n}_t \times \vec{n}_{\bar{t}})$ and the sign of this TP is determined by the quantity $(\vec{t} - \vec{\bar{t}}) \cdot (\vec{n}_t \times \vec{n}_{\bar{t}})$. **(KK: try to connect previous sentences to something later on. . . .)** The values obtained for the asymmetry associated with this TP are shown in Table II. By comparing the results in Tables I and II, we see that the capability of this asymmetry to distinguish between the two CP-mixed hypotheses is increased by at least 3σ.

TABLE II: Asymmetry for the TP ϵ_4 for the SM case and the two CP-mixed cases defined by $\kappa_t = 1, \tilde{\kappa}_t = \pm 1$. The values are obtained by using 10^5 simulated events.

κ_t	$\tilde{\kappa}_t$	$\mathcal{A}(\epsilon_4)$	$\mathcal{A}(\epsilon_4)/\sigma_{\mathcal{A}}$
1	-1	-0.0371	-12
1	0	0.0004	0.1
1	1	0.0461	14

Finally, it is worth noting that the asymmetries described in this subsection are not useful for discriminating between the SM hypothesis ($\kappa_t = 1, \tilde{\kappa}_t = 0$) and the pure pseudoscalar hypothesis ($\kappa_t = 0, \tilde{\kappa}_t = 1$). Since the numerators of the asymmetries are all linear in both κ_t and $\tilde{\kappa}_t$, they

are expected to vanish in these cases. However, we will show in the next subsection that there exist angular distributions derived from the TPs that are actually suitable for distinguishing between these two hyphotheses.

B. Angular Distributions

Given a certain TP, it is possible to define associated angular distributions that are sensitive to the pseudoscalar coupling $\tilde{\kappa}_t$. In order to clarify this, let us first consider the TP $\epsilon(t, \bar{t}, n_t, n_{\bar{t}})$. This TP can be written as $\epsilon(t + \bar{t}, \bar{t}, n_t, n_{\bar{t}})$, so that in the reference frame defined by $\vec{t} + \vec{\bar{t}} = 0$ and $\vec{\bar{t}} \parallel \hat{z}$ we have

$$\epsilon(t + \bar{t}, \bar{t}, n_t, n_{\bar{t}}) = M_{t\bar{t}} \, |\vec{\bar{t}}| \, (\vec{n}_t \times \vec{n}_{\bar{t}})_z = M_{t\bar{t}} \, |\vec{\bar{t}}| |\vec{n}_t| |\vec{n}_{\bar{t}}| \sin\theta_{n_t} \sin\theta_{n_{\bar{t}}} \sin\Delta\phi(n_t, n_{\bar{t}}), \tag{28}$$

where $M_{t\bar{t}}$ is the invariant mass of the $t\bar{t}$ pair, the angles θ_{n_t} and $\theta_{n_{\bar{t}}}$ denote the polar angles of $\vec{n}_t$ and $\vec{n}_{\bar{t}}$, respectively, and $\Delta\phi(n_t, n_{\bar{t}})$ is the angular difference between the projections of $\vec{n}_t$ and $\vec{n}_{\bar{t}}$ onto the plane perpendicular to $\vec{\bar{t}}$. If we define the angle $\Delta\phi(n_t, n_{\bar{t}})$ to be within the range $[-\pi, \pi]$, we see from Eq. (28) that its sign will determine the sign of the TP. Thus, the distribution of the number of events with respect to the angle $\Delta\phi(n_t, n_{\bar{t}})$ is related to the asymmetry of the TP,

$$\mathcal{A}(\epsilon) = 1 - 2\frac{N(\epsilon < 0)}{N_T} \quad \text{and} \quad \frac{N(\epsilon < 0)}{N_T} = \int_{-\pi}^{0} \frac{1}{N_T} \frac{dN}{d\Delta\phi(n_t, n_{\bar{t}})} \, d\Delta\phi(n_t, n_{\bar{t}}), \tag{29}$$

where N_T is the total number of events. **(KK: Have we checked numerically that the above expression does indeed hold numerically for the various distributions? It's an exact relation, correct?)** Moreover, for a certain TP one can derive different angular distributions by considering different reference frames, although all of these will satisfy Eq. (29) (note that $\mathcal{A}(\epsilon)$ is Lorentz invariant). Recalling the various TPs considered in Sec. II, we examine the following angular distributions.

1. $\boldsymbol{\epsilon_1 = \epsilon(t, \bar{t}, n_t, n_{\bar{t}})}$. To probe ϵ_1, we construct the distribution $d\sigma/d\Delta\phi_1(n_t, n_{\bar{t}})$ in the rest frame of $t\bar{t}$, taking $\vec{\bar{t}}$ to define the z-axis. The angle $\Delta\phi_1(n_t, n_{\bar{t}})$ is the angular difference between the projection of the spin vectors in the plane perpendicular to $\vec{\bar{t}}$.

2. $\boldsymbol{\epsilon_2 = \epsilon(Q, \bar{t}, n_t, n_{\bar{t}})}$. In this case, we define the distribution $d\sigma/d\Delta\phi_2(n_t, n_{\bar{t}})$ in the rest frame of Q, taking $\vec{\bar{t}}$ to define the z-axis. The angle $\Delta\phi_2(n_t, n_{\bar{t}})$ is the angular difference between the projection of the spin vectors in the plane perpendicular to $\vec{\bar{t}}$.

3. $\boldsymbol{\epsilon_3 = \epsilon(Q, t, n_t, n_{\bar{t}})}$. The distribution $d\sigma/d\Delta\phi_3(n_t, n_{\bar{t}})$ is also defined in the rest frame of Q, but this time taking $\vec{t}$ to be along the z-axis. The angle $\Delta\phi_3(n_t, n_{\bar{t}})$ is the angular difference between the projection of the spin vectors in the plane perpendicular to $\vec{\bar{t}}$.

Figure 5 shows the normalized distributions obtained for the first case listed above. Four scenarios are considered, corresponding to the SM ($\kappa_t = 1$ and $\tilde{\kappa}_t = 0$), two cases in which the Higgs boson has mixed CP couplings ($\kappa_t = 1$ and $\tilde{\kappa}_t = \pm 1$) and a case in which the Higgs boson is purely CP-odd ($\kappa_t = 0, \tilde{\kappa}_t = 1$). Figure 6 shows the analogous distributions for ϵ_2. The distributions corresponding to ϵ_3 are similar to those of ϵ_2, except that the "shifts" are in

the opposite directions for the two mixed-CP cases. Given the similarities of the plots we do not include them here. **(KK: did I reword this correctly?)**

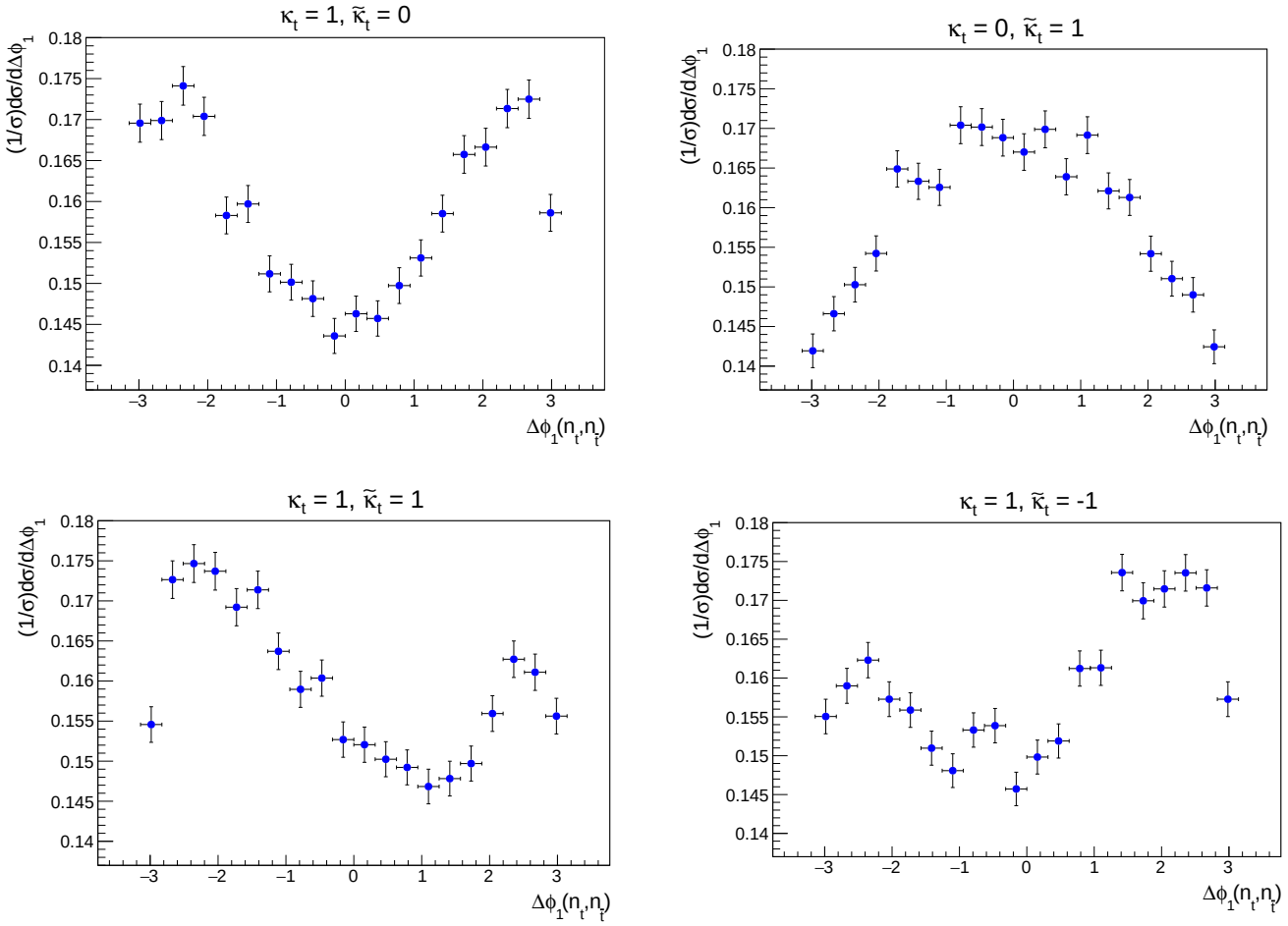

FIG. 5: Angular distributions associated with the TP $\epsilon_1 = \epsilon(t, \bar{t}, n_t, n_{\bar{t}})$ for various values of κ_t and $\tilde{\kappa}_t$. The error bars correspond to the statistical uncertainties.

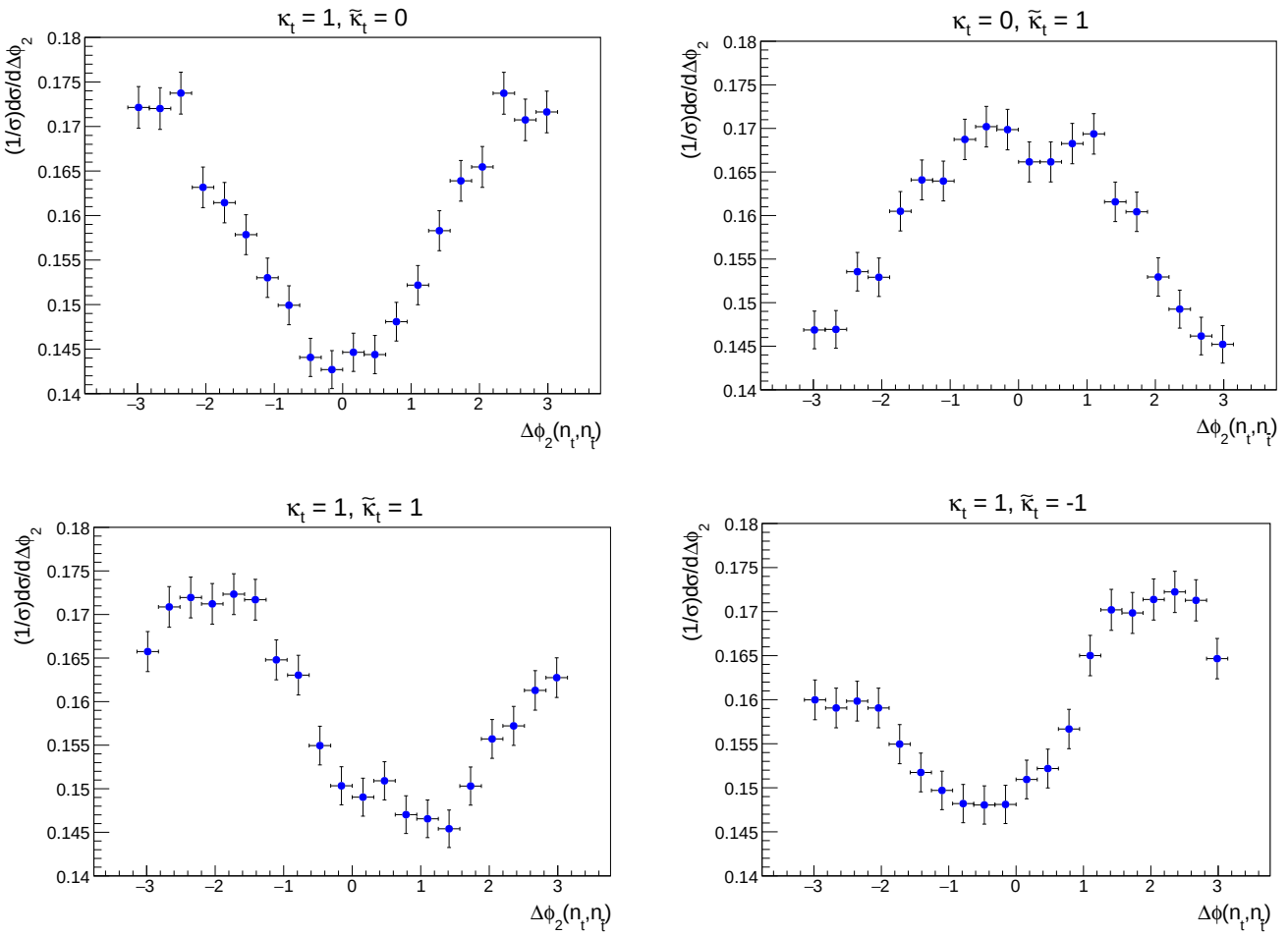

FIG. 6: Angular distributions associated with the TP $\epsilon_2 = \epsilon(Q, \bar{t}, n_t, n_{\bar{t}})$ for various values of κ_t and $\tilde{\kappa}_t$. The error bars indicate the statistical uncertainties.

As can be seen from Figs. 5 and 6, the peaks of the distributions are shifted to the left or the right of the origin in the mixed-CP cases ($\kappa_t = 1$ and $\tilde{\kappa}_t = \pm 1$). The magnitude of the shift appears to be approximately the same in both cases, but is in the opposite direction for $\kappa_t = \tilde{\kappa}_t = 1$ compared to $\kappa_t = -\tilde{\kappa}_t = 1$, thus allowing one to distinguish the sign of the pseudoscalar coupling. The observed dependence on the sign of $\tilde{\kappa}_t$ in these cases is consistent with the fact that the numerator of $\mathcal{A}(\epsilon)$ is linear in $\tilde{\kappa}_t$ [see Eq. (26)] and that the quantity $N(\epsilon < 0)/N_T$ is related to the angular distribution according to Eq. (29). The angular distributions for the SM case ($\kappa_t = 1$ and $\tilde{\kappa}_t = 0$) and the pure pseudoscalar case ($\kappa_t = 0$ and $\tilde{\kappa}_t = 1$) are visibly different from each other and from the mixed-CP scenarios. Comparing the SM and purely pseudoscalar cases, we note that while the angular distributions for the former case exhibit a minimum at $\Delta\phi_{1,2}(n_t, n_{\bar{t}}) = 0$, those for the latter case exhibit a peak at this location. Thus, these two scenarios can be distinguished from each other via these angular distributions. This is to be contrasted with the situation for the asymmetries $\mathcal{A}(\epsilon)$, which vanish in both cases.

In order to quantify the shifts discussed above, we have fitted the simulated distributions

with the following function, which was proposed in Ref. [14],

$$\frac{1}{\sigma}\frac{d\sigma}{d\Delta\phi_i(n_t, n_{\bar{t}})} = a_0 + a_1 \cos(\Delta\phi_i(n_t, n_{\bar{t}}) + \delta), \qquad i = 1, 2, 3. \tag{30}$$

To the extent that the above expression is exact, we note that Eq. (29) **(KK: corrected the equation number; please check...)** gives $\mathcal{A}(\epsilon_i) = 4a_1 \sin\delta$. With this fitting function, we obtain phase shifts δ that are approximately between 0.9 and 1 (-1 and -0.9) for $\kappa_t = \tilde{\kappa}_t = 1$ ($\kappa_t = -\tilde{\kappa}_t = 1$) both for ϵ_1 and ϵ_2. However, the quality of the fits is not very good, particularly for ϵ_1. The χ^2/d.o.f for the fits in this case are in the range 1.69-3.86, while for ϵ_2 they are in the range 0.53-1.16. **(KK: Did we do 4 fits for each ϵ? Or only 2? If only 2, maybe saying "in the range" is not quite correct, since the two data points are simply the endpoints of the "range". If the range includes all 4 fits for each, maybe we could state that explicitly, since the preceding sentences are only discussing the two mixed-CP scenarios.)** The leading source of the deviation from the functional form proposed in Eq. (30) appears to be the ΔR_{ll} cut that we have imposed. In fact, when this cut is turned off, the above ranges for χ^2/d.o.f become 0.75-1.14 and 0.44-1.07 for the ϵ_1 and ϵ_2 distributions, respectively. Tables III and IV list the results of the fits obtained when the $\Delta R_{\ell\ell}$ cut is relaxed. Also, Fig. 7 shows the angular distributions, along with the fit curves, for the CP-mixed cases with the $\Delta R_{\ell\ell}$ cut turned off. The results for the TP ϵ_3 are relatively similar to those for ϵ_2, except that the phase shifts have the opposite sign in the CP-mixed cases. Given this similarity we do not include the results for the ϵ_3 distribution here.

TABLE III: Fit results for the angular distribution $d\sigma/(\sigma d\Delta\phi_1(n_t, n_{\bar{t}}))$ (related to the TP $\epsilon_1 = \epsilon(t, \bar{t}, n_t, n_{\bar{t}})$) with the $\Delta R_{\ell\ell}$ cut turned off. Note that the sign of the parameter a_1 changes for $\kappa_t = 0, \kappa_t = 1$, compared to the other cases. **(KK: Do we restrict δ to be between $\pm\pi/2$? If not, we could require a_1 to always be positive, and absorb the sign change by a shift of δ by π or ssomething. Maybe we should clarify the range allowed for δ.)**

κ_t	$\tilde{\kappa}_t$	a_0	a_1	δ
1	-1	0.1592 ± 0.0006	-0.0139 ± 0.0008	0.81 ± 0.07
1	0	0.1595 ± 0.0006	-0.0181 ± 0.0008	0.002 ± 0.06
1	1	0.1591 ± 0.0006	-0.0131 ± 0.0008	-0.82 ± 0.07
0	1	0.1591 ± 0.0006	0.0102 ± 0.0008	0.11 ± 0.08

TABLE IV: Fit results for the angular distribution $d\sigma/(\sigma d\Delta\phi_2(n_t, n_{\bar{t}}))$ (related to the TP $\epsilon_2 = \epsilon(Q, \bar{t}, n_t, n_{\bar{t}})$), with the $\Delta R_{\ell\ell}$ cut turned off. As was the case in Table III, the sign of the parameter a_1 changes for $\kappa_t = 0, \kappa_t = 1$.

κ_t	$\tilde{\kappa}_t$	a_0	a_1	δ
1	-1	0.1591 ± 0.0006	-0.0146 ± 0.0008	0.73 ± 0.06
1	0	0.1594 ± 0.0007	-0.0190 ± 0.0008	0.005 ± 0.06
1	1	0.1592 ± 0.0006	-0.0136 ± 0.0008	-0.77 ± 0.07
0	1	0.1591 ± 0.0006	0.0113 ± 0.0008	0.09 ± 0.08

From Tables III and IV we see that the parameter δ is sensitive not only to the modulus of $\tilde{\kappa}_t$ but also to its sign, as expected if Eq. (29) is taken into account. The phase shift δ for the distribution of the angle $\Delta\phi_1$ appears to exhibit a slightly higher sensitivity than that obtained from the $\Delta\phi_2$-distribution, albeit both are still compatible within the statistical uncertainties. However, it is important to stress that the fits of the $\Delta\phi_2$-distributions give allways smaller values for χ^2/d.o.f.

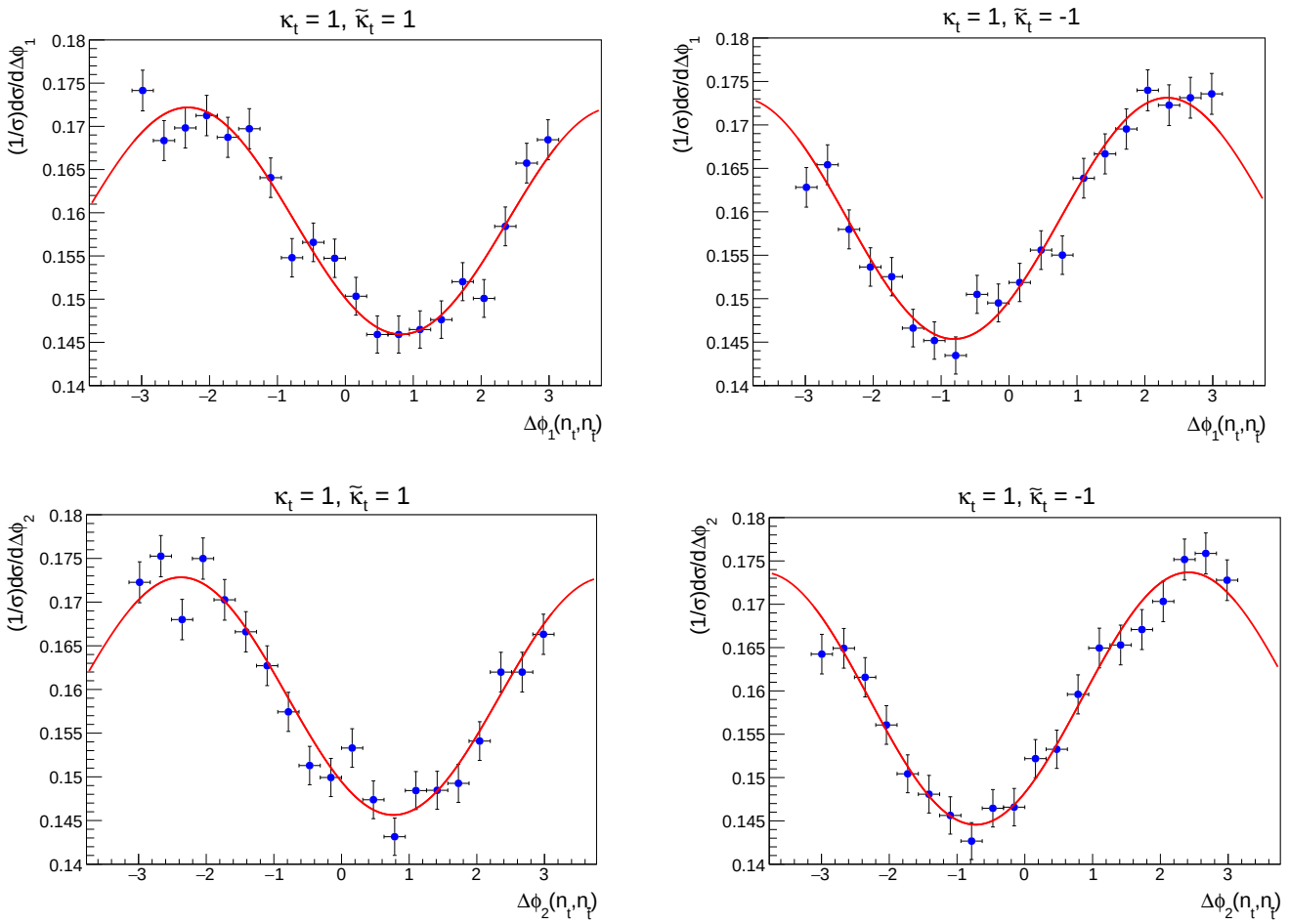

FIG. 7: Angular distributions $d\sigma/(\sigma d\Delta\phi_1(n_t, n_{\bar{t}}))$ (top) and $d\sigma/(\sigma d\Delta\phi_2(n_t, n_{\bar{t}}))$ (bottom) associated with the TPs $\epsilon_1 = \epsilon(t, \bar{t}, n_t, n_{\bar{t}})$ and $\epsilon_2 = \epsilon(Q, \bar{t}, n_t, n_{\bar{t}})$, respectively, for the CP-mixed cases $\kappa_t = \tilde{\kappa}_t = 1$ (left) and $\kappa_t = -\tilde{\kappa}_t = 1$ (right). The $\Delta R_{\ell\ell}$ cut was turned off when generating these results. The corresponding fit curves [see Eq. (30)] are displayed in red.

Concerning the angular distributions that can be related to the combination ϵ_4, we have analized the $\Delta\phi(n_t, n_{\bar{t}})$ distribution in the Q rest frame with H in the z-axis for various values of κ_t and $\tilde{\kappa}_t$. We have found that these distributions are not described by Eq. (30) and their range of variation is larger than that of the distributions displayed in Figs. 5 and 6. Unlike the distributions related to ϵ_1-ϵ_3, those arising from ϵ_4 exhibit small changes in their shapes for all the considered hypotheses and for this reason we have not included the corresponding plots here. However, the larger range of variation of the ϵ_4 distributions leads to higher values for the asymmetry (as can be sees from Tables I and II) even when the changes in the respective shapes are smaller than in the case of the distributions described by Eq. (30).

C. Mean value

We turn now to consider the last type of observables constructed from the TPs that are sensitive to $\tilde{\kappa}_t$, the mean value. Given a certain TP, we define its mean value in the following manner,

$$\langle \epsilon \rangle = \frac{\int \epsilon \, \{ d\sigma(pp \to b\,\ell^+\nu_\ell\,\bar{b}\,\ell^-\bar{\nu}_\ell H)/d\Phi \}\, d\Phi}{\int \{ d\sigma(pp \to b\,\ell^+\nu_\ell\,\bar{b}\,\ell^-\bar{\nu}_\ell H)/d\Phi \}\, d\Phi}, \tag{31}$$

where Φ is the Lorentz invariant phase space corresponding to the final state $b\,\ell^+\nu_\ell\,\bar{b}\,\ell^-\bar{\nu}_\ell H$. From Eq. (20) we see that only the terms linear in κ_t and $\tilde{\kappa}_t$ will contribute to the mean value, so that we expect this observable to be sensitive not only to the value but also to the relative sign of the couplings.

The results obtained for the TPs $\epsilon_1 = \epsilon(t, \bar{t}, n_t, n_{\bar{t}})$, $\epsilon_2 = \epsilon(Q, \bar{t}, n_t, n_{\bar{t}})$ and $\epsilon_3 = \epsilon(Q, t, n_t, n_{\bar{t}})$ introduced in Sec. II are displayed in Table V, where we list the deviation of the mean values from the SM case ($\tilde{\kappa}_t = 0$) in terms of the corresponding statistical uncertainty of the estimator of $\langle \epsilon \rangle$, $\bar{\epsilon}$.

TABLE V: Mean values obtained for the TPs $\epsilon_{1,2,3}$ for the SM case and two CP-mixed cases with opposite sign in the pseudoscalar coupling. The values are obtained by using 10^5 simulated events.

κ_t	$\tilde{\kappa}_t$	$\langle\epsilon_1\rangle/\sigma_{\bar{\epsilon}_1}$	$\langle\epsilon_2\rangle/\sigma_{\bar{\epsilon}_2}$	$\langle\epsilon_3\rangle/\sigma_{\bar{\epsilon}_3}$
1	-1	4.26	4.94	-5.81
1	0	-0.91	-0.22	1.25
1	1	-7.98	-8.83	8.75

We see that the three observables are capable of disinguishing the SM case from both CP-mixed cases. Further, the observables are sensitive to the sign of $\tilde{\kappa}_t$ and the two CP-mixed cases are also clearly disentangled. The observables $\langle\epsilon_2\rangle$ and $\langle\epsilon_3\rangle$ appear to be slightly more sensitive than $\langle\epsilon_1\rangle$. On the other hand, the mean value for the combination ϵ_4 introduced in Sec. III A gives slightly smaller values than those listed in Table V, with $-4.32, 1.11$ and 7.23 for the cases $(\kappa_t = 1, \tilde{\kappa}_t = -1, 0, 1)$ respectively. As with the asymmetry, the hypotheses CP-even and CP-odd cannot be distinguished by the mean value that is also linear in both κ_t and $\tilde{\kappa}_t$ (see Eqs. (20) and (31)). By taking into account the results given in Sec. III A, we can conclude that the sensitivity to the NP contribution is smaller for the mean values than for the asymmetries of the TPs under consideration.

IV. CP-ODD OBSERVABLES NOT DEPENDING ON t AND $\bar{t}$ SPIN VECTORS

So far we have considered three TPs involving the momenta $t, \bar{t}$ and Q and the spin vectors n_t and $n_{\bar{t}}$ given in Eqs. (3)-(4). In fact, we have described the general form of the differential cross-section in terms of these vectors in Eq. (20). Here, we will take into account another possibilities

for the choice of the vectors from which the CP-odd observables can be constructed. From the definitions in Eqs. (3)-(4), we see that the TPs $\epsilon_{1,2,3}$ can be written as follows,

$$\epsilon(t,\bar{t},n_t,n_{\bar{t}}) = \frac{m_t^2}{(t\cdot\ell^+)(\bar{t}\cdot\ell^-)}\,\epsilon(t,\bar{t},\ell^-,\ell^+), \tag{32}$$

$$\epsilon(Q,\bar{t},n_t,n_{\bar{t}}) = \frac{m_t^2}{(t\cdot\ell^+)(\bar{t}\cdot\ell^-)}\left(\epsilon(t,\bar{t},\ell^-,\ell^+)+\epsilon(H,\bar{t},\ell^-,\ell^+)+\frac{(t\cdot\ell^+)}{m_t^2}\epsilon(H,\bar{t},t,\ell^-)\right) \tag{33}$$

$$\epsilon(Q,t,n_t,n_{\bar{t}}) = \frac{m_t^2}{(t\cdot\ell^+)(\bar{t}\cdot\ell^-)}\left(-\epsilon(t,\bar{t},\ell^-,\ell^+)+\epsilon(H,t,\ell^-,\ell^+)+\frac{(\bar{t}\cdot\ell^-)}{m_t^2}\epsilon(H,\bar{t},t,\ell^+)\right). \tag{34}$$

The above equations express the TPs studied in the last sections as linear combination of TPs involving the momenta $t,\bar{t},H,\ell^+$ and ℓ^-, with coefficients that are functions of phase space variables. These five momenta give rise to five TPs whose sensitivity can also be tested by means of the observables introduced in Secs. III A-III C. In the first place, we have found that TPs not including both lepton and anti-lepton momenta present a negligible sensitivity, and then we will concentrate here on the results obtained for the remaining TPs, $\epsilon_5 \equiv \epsilon(t,\bar{t},\ell^-,\ell^+), \epsilon_6 \equiv \epsilon(H,t,\ell^-,\ell^+)$ and $\epsilon_7 \equiv \epsilon(H,\bar{t},\ell^-,\ell^+)$. The Tables VI and VII summarize the results for these TPs.

TABLE VI: Mean values obtained for the TPs $\epsilon_{5,6,7}$ for the SM case and two CP-mixed cases with opposite sign in the pseudoscalar coupling. The values correspond to 10^5 simulated events.

κ_t	$\tilde{\kappa}_t$	$\langle\epsilon_5\rangle/\sigma_{\bar{\epsilon}_5}$	$\langle\epsilon_6\rangle/\sigma_{\bar{\epsilon}_6}$	$\langle\epsilon_7\rangle/\sigma_{\bar{\epsilon}_7}$
1	−1	3.98	−1.96	1.69
1	0	−0.43	1.25	0.74
1	1	−6.76	3.46	−3.29

TABLE VII: Asymmetries for the TPs $\epsilon_{5,6,7}$ for the SM case and the two CP-mixed cases defined by $\kappa_t = 1, \tilde{\kappa}_t = \pm 1$. The values correspond to 10^5 simulated events.

κ_t	$\tilde{\kappa}_t$	$\mathcal{A}(\epsilon_5)$	$\mathcal{A}(\epsilon_5)/\sigma_{\mathcal{A}}$	$\mathcal{A}(\epsilon_6)$	$\mathcal{A}(\epsilon_6)/\sigma_{\mathcal{A}}$	$\mathcal{A}(\epsilon_7)$	$\mathcal{A}(\epsilon_7)/\sigma_{\mathcal{A}}$
1	−1	0.0315	10.0	−0.0134	−4.2	0.0111	3.5
1	0	−0.0021	−0.7	−0.0011	−0.3	0.0009	0.3
1	1	−0.0379	−12.0	0.0143	4.5	−0.0137	−4.3

We see that the TP ϵ_5 gives rise to asymmetries and mean values that are clearly higher than those obtained from ϵ_6 and ϵ_7. This is in contrast to the TPs $\epsilon_{1,2,3}$, for which the asymmetries and mean values are comparable (see Tables I and V). We also note that the asymmetry for ϵ_5 is exactly the same as for ϵ_1 as was expected from Eq. (32) since the proportionality factor relating them is positive definite. Regarding the mean values, we see by comparing Tables V and VI that the TPs $\epsilon_{1,2,3}$ appear to have a higher sensitivity to the pseudoscalar coupling than $\epsilon_{5,6,7}$.

It is important to mention that in the $t\bar{t}$ rest frame the sign of the TP ϵ_5 is defined through the angle $\Delta\phi_{\ell^-\ell^+}$ (recall the discussion on Eq. (31)), which is the angular difference between the projections of the leptons momenta onto the plane perpendicular to $\vec{t}$. By a similar argument to that discussed at the beginning of Sec. III B, we can construct an associated angular distribution that, being constrained by the $\mathcal{A}(\epsilon_5)$, will be also sensitive to the sign of the pseudoscalar coupling. This angular variable is nothing but that proposed in [14] as a useful CP-odd observable. Moreover, it is shown in [14] that this angular distribution follows the functional form given in Eq. (30). Due to the fact that this distribution is constrained by $\mathcal{A}(\epsilon_5)$ which is equal to $\mathcal{A}(\epsilon_1)$ and smaller than $\mathcal{A}(\epsilon_{2,3})$, the corresponding shifts (δ) obtained for different values of $\tilde{\kappa}_t$ are expected to be of the same order than those exhibited by the $\Delta\phi_1(n_t, n_{\bar{t}})$ distribution and somewhat smaller than those observed in the $\Delta\phi_2(n_t, n_{\bar{t}})$ distribution.

In analogy to the combination of TPs considered in Sec. III, we have found a combination of the TPs $\epsilon_{5,6,7}$ for which the asymmetry is enhanced with respect to ϵ_5-ϵ_7,

$$\epsilon_8 = 2\epsilon_5 - \epsilon_6 + \epsilon_7 = \epsilon(t + \bar{t} + H, t - \bar{t}, \ell^+, \ell^-). \tag{35}$$

We see from Eq. (35) that in the $t\bar{t}H$ rest frame $\epsilon_8 = M_{t\bar{t}H}(\vec{t} - \vec{\bar{t}}) \cdot (\vec{\ell}^+ \times \vec{\ell}^-)$, where $M_{t\bar{t}H}$ is the invariant mass of the system $t\bar{t}H$. Hence, in this reference frame the sign of the combination ϵ_8 is set by the quantity $(\vec{t} - \vec{\bar{t}}) \cdot (\vec{\ell}^+ \times \vec{\ell}^-)$. Taking into account Eqs. (27) and (35) along with the definition $Q = (t + \bar{t} + H)/2$, we see that the only relevant difference between ϵ_4 and ϵ_8 is that in the latter the spin vectors n_t and $n_{\bar{t}}$ have been replaced by the momenta of the leptons ℓ^+ and ℓ^- respectively. The values obtained for $\mathcal{A}(\epsilon_8)$ are shown in Table VIII. Compared to the TPs ϵ_5-ϵ_7 and ϵ_1, ϵ_3 (see Tables I and VII), the chosen combination exhibits a slightly higher sensitivity in the asymmetry for resolving the CP-mixed cases. This is not true in the case of the TPs ϵ_2 and ϵ_4, for which the asymmetry is larger (see Tables I, II and VIII). In particular, the comparison between ϵ_4 and ϵ_8 indicates that the use of the momenta of the leptons instead of the spin vectors produces a decrease in the sensitivity of the asymmetry.

From the TPs ϵ_5-ϵ_7 one can derive various angular distributions in the same manner we have discussed in Sec. III B for ϵ_1-ϵ_3. Of course, in this case the corresponding angle will be defined in terms of the momenta of the leptons instead of using the spin vectors. These distributions have the same behaviour than those derived from ϵ_1-ϵ_3, but only the shift obtained in the case of ϵ_5 is compatible to the values given in Tables for ϵ_1-ϵ_3. The shifts resulting from the fit of the distributions related to ϵ_6 and ϵ_7 are smaller. Taking into account these facts we do not give further details of the angular distributions for the TPs discussed in this section.

The mean value of ϵ_8 for the hypotheses under consideration is comparable with the values listed in Table VI for ϵ_5. Concerning the associated angular distributions, their range of variation is larger than in the case of the distributions related to ϵ_5-ϵ_7 but exhibit smaller changes in their shapes for the different hypothesis and for this reason we do not include here the corresponding plots.

TABLE VIII: Asymmetry for the TP ϵ_8 for the SM case and the two CP-mixed cases defined by $\kappa_t = 1, \tilde{\kappa}_t = \pm 1$. The values are obtained with 10^5 simulated events.

κ_t	$\tilde{\kappa}_t$	$\mathcal{A}(\epsilon_8)$	$\mathcal{A}(\epsilon_8)/\sigma_{\mathcal{A}}$
1	-1	0.0331	10.5
1	0	0.0023	0.7
1	1	-0.0403	-12.7

V. CP-ODD OBSERVABLES NOT DEPENDING ON t AND $\bar{t}$ MOMENTA

All the observables discussed in the above sections involve the momenta of the top and anti-top quarks thus requiring the full reconstruction of the kinematics of the individual t and $\bar{t}$ systems in order to be measured. Although challenging due to the presence of two neutrinos in the final state, this can be in principle done by applying a kinematic reconstruction method such that the neutrino weighting technique [25, 26]. Another possibility is to define observables that are not dependent on the t and $\bar{t}$ momenta but make use of the quarks b and $\bar{b}$. In order to construct such observables we will modify here the most sensitive observables studied in Secs. III and IV, namely the combinations ϵ_4 and ϵ_8 respectively. Let us first consider the combination ϵ_8 defined in Eq. (35) and replace the top and antitop momenta by the bottom and antibottom momenta respectively. Thus, we define

$$\epsilon_9 = \epsilon(b + \bar{b} + H, b - \bar{b}, \ell^+, \ell^-). \tag{36}$$

Note that now the sign of the TP ϵ_9 is set by the sign of the quantity $(\vec{b} - \vec{\bar{b}}) \cdot (\vec{\ell}^+ \times \vec{\ell}^-)$ in the $b\bar{b}H$ rest frame. This quantity is in fact used in [10] but in the lab frame in order to define a CP-odd observable that only depends on lab frame variables. The values of the asymmetry for ϵ_9 are listed in Table IX. By comparing Tables VIII and IX we see that the use of the $b, \bar{b}$ instead of $t, \bar{t}$ leads to a decrese in the sensitivity of the asymmetry by $\sim 5\sigma$ for $\kappa_t = 1, \tilde{\kappa}_t = \pm 1$. However, the observable is still capable of discriminating not only between the two CP-mixed hypotheses but also between these and the SM case. We proceed now in a similar way with the combination ϵ_4. By using Eq. (27) along with the definitions of the spin vectors in Eqs. (3)-(4), we can write

$$\epsilon_4 = \frac{m_t^2}{(t \cdot \ell^+) \cdot (\bar{t} \cdot \ell^-)} \epsilon(Q, t - \bar{t}, \ell^-, \ell^+) + \frac{1}{(t \cdot \ell^+)} \epsilon(Q, t, \ell^+, \bar{t}) - \frac{1}{(\bar{t} \cdot \ell^-)} \epsilon(Q, \bar{t}, t, \ell^-). \tag{37}$$

Since the asymmetry is not changed by an overall positive definite factor, we will concentrate on the following combination arising from the expression in Eq. (37),

$$\epsilon(Q, t - \bar{t}, \ell^-, \ell^+) + \frac{(\bar{t} \cdot \ell^-)}{m_t^2} \epsilon(Q, t, \ell^+, \bar{t}) - \frac{(t \cdot \ell^+)}{m_t^2} \epsilon(Q, \bar{t}, t, \ell^-), \tag{38}$$

TABLE IX: Asymmetry for the TP ϵ_9 for the SM case and the two CP-mixed cases defined by $\kappa_t = 1, \tilde{\kappa}_t = \pm 1$. The values are obtained with 10^5 simulated events.

κ_t	$\tilde{\kappa}_t$	$\mathcal{A}(\epsilon_9)$	$\mathcal{A}(\epsilon_9)/\sigma_{\mathcal{A}}$
1	-1	0.0171	5.4
1	0	0.0010	0.3
1	1	-0.0247	-7.8

and instead of replacing t and $\bar{t}$ directly by b and $\bar{b}$, we use their visible parts, namely $b + \ell^+$ and $\bar{b} + \ell^-$ respectively. This results in the following definition

$$\epsilon_{10} = \epsilon(\tilde{Q}, c_{b\bar{b}}\,, \ell^-, \ell^+) - w_1\,\epsilon(\tilde{Q}, b, \bar{b}, \ell^+) + w_2\,\epsilon(\tilde{Q}, b, \bar{b}, \ell^-), \tag{39}$$

where $\tilde{Q} \equiv (b+\ell^+ + \bar{b} + \ell^-)/2$ stands for the visible part of Q, $c_{b\bar{b}} = (1-w_1)\,b - (1-w_2)\,\bar{b}$ and the weights $w_{1,2}$ are given by $(\bar{b}\cdot\ell^-)/m_t^2$ and $(b\cdot\ell^+)/m_t^2$ respectively. Also, the contribution m_ℓ^2/m_t^2 has been neglected both in w_1 and in w_2. Note that if we set $w_1 = w_2 = 0$, the combination ϵ_{10} reduces to $\epsilon_9/2$ and $\mathcal{A}(\epsilon_{10})$ becomes equal to $\mathcal{A}(\epsilon_9)$. The results obatined for the asymmetry of ϵ_{10} are given in Table X. By comparing Tables II and X we see again that the sensitivity of the asymmetry decreases when t and $\bar{t}$ are not included in the TP. Nevertheless, the combination ϵ_{10} remains a useful observable for discriminating the CP nature of the Higgs boson, with the corresponding asymmetry having a sensitivity even higher than that of ϵ_9, as can be checked by taking into account Tables IX and X. More precisely, the separation between the CP-mixed hypotheses is enhanced by about 3σ. This improvement in the asymmetry of ϵ_{10} with respect to ϵ_9 may be due to two facts. In the first place, as was pointed out in Sec. IV when comparing the TPs ϵ_4 and ϵ_8, the asymmetry appears to be higher when the spin vectors are used instead of the lepton momenta and we see from Eqs. (36) and (39) that ϵ_{10}, being obtained from ϵ_4, contains the information on the spin vectors, as opposed to ϵ_9 that depends directly on the lepton momenta because it is derived from ϵ_8. In the second place, in order to obtain ϵ_{10} we have replaced in the expression for ϵ_4 the top and antitop momenta by their visible part, while in the case of ϵ_9 the bottom and antibottom momenta have been used.

TABLE X: Asymmetry for the TP ϵ_{10} for the SM case and the two CP-mixed cases defined by $\kappa_t = 1, \tilde{\kappa}_t = \pm 1$. The values are obtained by using 10^5 simulated events.

κ_t	$\tilde{\kappa}_t$	$\mathcal{A}(\epsilon_{10})$	$\mathcal{A}(\epsilon_{10})/\sigma_{\mathcal{A}}$
1	-1	-0.0213	-6.7
1	0	0.0031	1.0
1	1	0.0300	9.5

By using our set of simulated events we have also tested, for comparison purposes, the asymmetry of the lab frame observable given in [10]. We have obtained that this observable appears to be slightly less sensitive than the combination ϵ_{10}, giving rise to a separation between the CP-mixed hypotheses smaller by about 1.4σ.

VI. EXPERIMENTAL FEASIBILITY

By considering the mild selection cuts introduced in Sec. III, the SM cross section for $pp \to t\,(\to b\ell^+\nu_\ell)\,\bar{t}\,\left(\to \bar{b}\ell^-\bar{\nu}_\ell\right)\,H$, $\ell = e, \mu$ at 14 TeV is $\sim 15.3\,\text{fb}$ and hence the number of events expected within the context of the HL-LHC is $\sim 15.3\,\text{fb} \times 3000\,\text{fb}^{-1} = 4.59 \times 10^4$. This number is expected to be even larger in the case of $\kappa_t = 1, \tilde{\kappa}_t \neq 0$ since the corresponding cross section is then higher than the SM one. By taking into account NLO corrections to the production process and considering a K-factor around 1.2 [27–29], the number of events can be raised up to $\sim 5.49 \times 10^4$. On the other hand, additional cuts as well as the efficiency related to the reconstruction of particles momenta will contribute to decrease this number. For instance, in order to obtain the asymmetry of ϵ_4, the t and $\bar{t}$ momenta need to be reconstructed. This is challenging not only due to the presence of two neutrinos in the final state which escape the detector undetected but also because final state objects need to be asocciated with the respective parent quark [25]. As was already mentioned in Sec. V, a possibility is to use the neutrino weighting technique along with the kinematic equations arising from kinematic constraints related to the top and W masses as well as from the energy-momentum conservation at each of the decay vertices involved in the process. Within the context of $t\bar{t}$ this procedure has been used, for instance, in order to obtain measurements of spin correlation [25] and charge asymmetry [26]. Also, events reconstructed with this technique has been used in [30] for analyzing angular distributions that are useful for discriminating the signal from the backgrounds in $t\bar{t}H(H \to b\bar{b})$. In all these cases the corresponding efficiency in the reconstruction of the momenta is up to $\sim 80\%$.

Based on the discussion given in the previous paragraph, we have simulated sets of $5\times10^4, 1\times 10^4$ and 5×10^3 events and recalculated the most sensitive observable, namely $\mathcal{A}(\epsilon_4)$, for each case. The results are displayed in Table XI, where it can be seen that for a number of events close to that roughly estimated above within the context of the HL-LHC, the observable is still sensitive to $\tilde{\kappa}_t$ allowing to separate the CP-mixed cases by 19σ. As expected, the sensitivity worsen as the number of events is reduced, but even with 5×10^3 events the separation between the CP-mixed hypotheses under consideration is around 6.5σ.

Although the combination ϵ_{10} discussed in Sec. V avoids the problem of reconstructing the top and antitop momenta, we have also considered the respective asymmetry obtained for more conservative numbers of events. In Table XII we show the results for $\mathcal{A}(\epsilon_{10})$ when the number of events is reduced from 5×10^4 to 1×10^4. We see in this case that even with 1×10^4 simulated events the observable is capable to discriminate the CP-mixed cases by 5.6σ.

Finally, it is important to mention that a realistic analysis of the sensistivity of the observables discussed in this paper requires the study of the impact of the backgrounds as well as the hadronization of the quarks in the final state and the effects of the detector. If we consider the dominant decay mode of the higgs, $H \to b\bar{b}$, in order to maximize the cross section of the process, the signature is given by 4 b-jets, two leptons and missing energy, while the main background arise from the production of $t\bar{t}$ in asocciation with additional jets, being the dominant source the production of $t\bar{t} + b\bar{b}$. By applying a small set of cuts it is shown in [31] that the

TABLE XI: Asymmetry for the TP ϵ_4 obtained by using $5\times10^4, 1\times10^4$ and 5×10^3 simulated events for the SM case and the two CP-mixed cases defined by $\kappa_t = 1, \tilde{\kappa}_t = \pm 1$.

κ_t	$\tilde{\kappa}_t$	$N_{\rm ev} = 5\times10^4$		$N_{\rm ev} = 1\times10^4$		$N_{\rm ev} = 5\times10^3$	
		$\mathcal{A}(\epsilon_4)$	$\mathcal{A}(\epsilon_4)/\sigma_{\mathcal{A}}$	$\mathcal{A}(\epsilon_4)$	$\mathcal{A}(\epsilon_4)/\sigma_{\mathcal{A}}$	$\mathcal{A}(\epsilon_4)$	$\mathcal{A}(\epsilon_4)/\sigma_{\mathcal{A}}$
1	−1	−0.0405	−9.1	−0.0426	−4.3	−0.0496	−3.5
1	0	0.0004	0.1	−0.0084	−0.8	−0.0004	−0.03
1	1	0.0443	9.9	0.0434	4.2	0.0420	3.0

TABLE XII: Asymmetry for the TP ϵ_{10} in the SM case and the two CP-mixed cases defined by $\kappa_t = 1, \tilde{\kappa}_t = \pm 1$ when the number of simulated events is reduced from 5×10^4 to 1×10^4.

κ_t	$\tilde{\kappa}_t$	$N_{\rm ev} = 5\times10^4$		$N_{\rm ev} = 1\times10^4$	
		$\mathcal{A}(\epsilon_{10})$	$\mathcal{A}(\epsilon_{10})/\sigma_{\mathcal{A}}$	$\mathcal{A}(\epsilon_{10})$	$\mathcal{A}(\epsilon_{10})/\sigma_{\mathcal{A}}$
1	−1	−0.0270	−6.0	−0.0184	−1.8
1	0	0.0022	0.5	−0.0086	−0.9
1	1	0.0313	7.0	0.0380	3.8

signal to background ratio is largely improved. On the other hand, a rigorous treatment of the backgrounds and their impact with respect to the signal is performed in [32] by using $20.3\,\text{fb}^{-1}$ of data at $\sqrt{s} = 8\,\text{TeV}$.

The results shown in tables XI and XII reveal that with 5×10^3 and 1×10^4 events respectively the observables $\mathcal{A}(\epsilon_4)$ and $\mathcal{A}(\epsilon_{10})$ are still useful for testing $\tilde{\kappa}_t$. Without considering the lack of events related to the experimental analysis, these numbers of events correspond to a luminosity around ~ 300 - $600\,\text{fb}^{-1}$ for the SM and even smaller for the CP-mixed cases due to the larger cross section. This range of luminosities is in principle achievable in the short term by the LHC. We note that in order to be fully conclusive about the required luminosity, it is important to include the effects of hadronization, detector resolution, reconstruction eficciencies and so forth. However, this kind of analysis is out of the scope of this paper.

VII. CONCLUSIONS

In this paper we have presented a collection of CP-odd observables based on triple product correlations that are useful for disentangling the relative sign between the scalar (κ_t) and a potential pseudoscalar ($\tilde{\kappa}_t$) top-Higgs couplings in the $t\bar{t}H$ production with both tops decaying

leptonically. We have tested the sensitivity of the proposed observables by considering three types of observables: asymmetries, mean values and angular distributions.

Through the use of spinor techniques we have written the expression for the differential cross section of the full process in such a manner that the production and the decay parts are separated, although connected by the spin vectors of the top and antitop which are given in terms of the momenta of the leptons in the final state. Moreover, we have indentified the terms linear in κ_t and $\tilde{\kappa}_t$ as those involving TPs. Among these, we have explored the three that do not involve the momenta of the incoming quarks/gluons and at the same time incorporate both spin vectors: $\epsilon_1 \equiv \epsilon(t, \bar{t}, n_t, n_{\bar{t}})$, $\epsilon_2 \equiv \epsilon(Q, \bar{t}, n_t, n_{\bar{t}})$ and $\epsilon_3 \equiv \epsilon(Q, t, n_t, n_{\bar{t}})$.

We have found that $\epsilon_{1,2,3}$ allow to distinguish between the CP-mixed hypotheses by more than $\sim 20\sigma$ in the case of asymmetries and $\sim 10\sigma$ in the case of mean values when 1×10^5 simulated events are used. Furthermore, we have shown that the angular distributions asocciated with these TPs are also sensitive to the value of κ_t and $\tilde{\kappa}_t$ exhibiting a phase shift that varies according to the values taken by these couplings. On the other hand, by exploring TPs that incorporate the momenta of the Higgs and the leptons instead of the spin vectors we can conclude that the observables studied here appear to be more sensitive when the spin vectors are used.

On the other hand, we have proposed a combination of the TPs considered in the first place, $\epsilon_4 \equiv \epsilon_3 - \epsilon_2$, that exhibits the highest sensitivity with the separation between the CP-mixed hypotheses being increased by at least 3σ in the asymmetry for 1×10^5 events with respect to $\mathcal{A}(\epsilon_{1,2,3})$. Again, when a similar combination is constructed by using the leptons momenta instead of the spin vectors (ϵ_8), the sensitivity in the asymmetry is decreased by $\sim 3\sigma$ compared to $\mathcal{A}(\epsilon_4)$ for the same number of events, giving values compatible with those obtained for the asymmetry of ϵ_2 and ϵ_3.

Taking into account the challenge of reconstructing the top and antitop momenta due to the presence of two neutrinos in the final state, we have proposed and tested two TP correlations that avoid this difficulty. The first one is obtained by replacing the t and $\bar{t}$ by the b and $\bar{b}$ momenta (ϵ_9), whereas the second includes the visible part of the t and $\bar{t}$ momenta (ϵ_{10}). We have encountered that the latter is the most sensitive leading to a discrimination of the CP-mixed cases under analysis by up to $\sim 16\sigma$.

Finally we have discussed the feasibility of the most sensitive observables proposed here. We have found that with 5×10^3 and 1×10^4 events respectively the observables $\mathcal{A}(\epsilon_4)$ and $\mathcal{A}(\epsilon_{10})$ are still useful for testing the hypotheses ($\kappa_t = 1, \tilde{\kappa}_t = \pm 1$) giving rise to separations of order $\sim 6\sigma$. These required number of events would be reachable in principle in the short term by the LHC and hence the capability of the observables studied here for testing the sign of $\tilde{\kappa}_t/\kappa_t$ could be probed in that context.

Acknowledgments This work has been partially supported by ANPCyT under grants No. PICT 2013-0433 and No. PICT 2013-2266, and by CONICET (NM, AS). The work of KK was supported by the U.S. National Science Foundation under Grant PHY-1215785. KK also acknowledges sabbatical support from Taylor University.

REFERENCES

[1] G. Aad *et al.* (ATLAS Collaboration), Physics Letters B **716**, 1 (2012).

[2] S. Chatrchyan *et al.* (CMS Collaboration), Physics Letters B **716**, 30 (2012).

[3] J. Brod, U. Haisch, and J. Zupan, Journal of High Energy Physics **2013**, 180 (2013), 10.1007/JHEP11(2013)180.

[4] J. Ellis and T. You, Journal of High Energy Physics **2013**, 103 (2013), 10.1007/JHEP06(2013)103.

[5] A. Djouadi and G. Moreau, The European Physical Journal C **73**, 2512 (2013), 10.1140/epjc/s10052-013-2512-9.

[6] K. Cheung, J. Lee, and P.-Y. Tseng, Journal of High Energy Physics **2013**, 134 (2013), 10.1007/JHEP05(2013)134.

[7] J. Baron *et al.* (ACME Collaboration), Science **343**, 269 (2014).

[8] R. Harnik, A. Martin, T. Okui, R. Primulando, and F. Yu, Phys. Rev. D **88**, 076009 (2013).

[9] M. Farina, C. Grojean, F. Maltoni, E. Salvioni, and A. Thamm, Journal of High Energy Physics **2013**, 22 (2013), 10.1007/JHEP05(2013)022.

[10] F. Boudjema, D. Guadagnoli, R. M. Godbole, and K. A. Mohan, Phys. Rev. D **92**, 015019 (2015); M. R. Buckley and D. Goncalves, (2015), arXiv:1507.07926 [hep-ph]; G. Li, H.-R. Wang, and S.-h. Zhu, (2015), arXiv:1506.06453 [hep-ph]; Y. Chen, D. Stolarski, and R. Vega-Morales, Phys. Rev. **D92**, 053003 (2015), arXiv:1505.01168 [hep-ph]; S. Khatibi and M. M. Najafabadi, *ibid.* **D90**, 074014 (2014), arXiv:1409.6553 [hep-ph].

[11] J. F. Gunion and X.-G. He, Phys. Rev. Lett. **76**, 4468 (1996); J. F. Gunion, B. Grzadkowski, and X.-G. He, *ibid.* **77**, 5172 (1996); J. F. Gunion and J. Pliszka, Physics Letters B **444**, 136 (1998); X.-G. He, G.-N. Li, and Y.-J. Zheng, International Journal of Modern Physics A **30**, 1550156 (2015).

[12] G. Mahlon and S. Parke, Phys. Rev. D **53**, 4886 (1996); Physics Letters B **411**, 173 (1997); Phys. Rev. D **81**, 074024 (2010); D. Atwood, A. Aeppli, and A. Soni, Phys. Rev. Lett. **69**, 2754 (1992).

[13] S. Biswas, R. Frederix, E. Gabrielli, and B. Mele, Journal of High Energy Physics **2014**, 20 (2014), 10.1007/JHEP07(2014)020.

[14] J. Ellis, D. Hwang, K. Sakurai, and M. Takeuchi, Journal of High Energy Physics **2014**, 4 (2014), 10.1007/JHEP04(2014)004.

[15] O. Antipin and G. Valencia, Phys. Rev. D **79**, 013013 (2009); G. Valencia, *Proceedings on 11th International Conference on Heavy Quarks and Leptons (HQL 2012)*, PoS **HQL2012**, 050 (2012), arXiv:1301.0962 [hep-ph].

[16] A. Hayreter and G. Valencia, Phys. Rev. D **88**, 034033 (2013).

[17] T. Arens and L. M. Sehgal, Phys. Rev. D **50**, 4372 (1994).

[18] S. Kawasaki, T. Shirafuji, and S. Y. Tsai, Prog. Theor. Phys. **49**, 1656 (1973).

[19] P. Saha, K. Kiers, B. Bhattacharya, D. London, A. Szynkman, and J. Melendez, (2015),

arXiv:1510.00204 [hep-ph]; P. Saha, K. Kiers, D. London, and A. Szynkman, Phys. Rev. **D90**, 094016 (2014), arXiv:1407.1725 [hep-ph]; K. Kiers, P. Saha, A. Szynkman, D. London, S. Judge, and J. Melendez, **D90**, 094015 (2014), arXiv:1407.1724 [hep-ph]; K. Kiers, T. Knighton, D. London, M. Russell, A. Szynkman, and K. Webster, **D84**, 074018 (2011), arXiv:1107.0754 [hep-ph].

[20] R. Kleiss and W. Stirling, Nuclear Physics B **262**, 235 (1985).

[21] M. L. Mangano and S. J. Parke, Physics Reports **200**, 301 (1991).

[22] H. W. Fearing and S. Scherer, Phys. Rev. D **53**, 315 (1996).

[23] W. Bernreuther, A. Brandenburg, Z. Si, and P. Uwer, Nuclear Physics B **690**, 81 (2004).

[24] J. Alwall, R. Frederix, S. Frixione, V. Hirschi, F. Maltoni, O. Mattelaer, H.-S. Shao, T. Stelzer, P. Torrielli, and M. Zaro, Journal of High Energy Physics **2014**, 79 (2014), 10.1007/JHEP07(2014)079.

[25] *Measurements of spin correlation in top-antitop quark events from proton-proton collisions at s = 7 TeV using the ATLAS detector*, Tech. Rep. ATLAS-CONF-2013-101 (CERN, Geneva, 2013).

[26] G. Aad *et al.* (ATLAS Collaboration), Journal of High Energy Physics **2015**, 61 (2015), 10.1007/JHEP05(2015)061.

[27] S. Dawson, L. H. Orr, L. Reina, and D. Wackeroth, Phys. Rev. D **67**, 071503 (2003).

[28] W. Beenakker, S. Dittmaier, M. Kramer, B. Plumper, M. Spira, and P. Zerwas, Nuclear Physics B **653**, 151 (2003).

[29] S. Dittmaier *et al.* (LHC Higgs Cross Section Working Group), *Handbook of LHC Higgs Cross Sections: 1. Inclusive Observables* (CERN, Geneva, 2011).

[30] S. P. Amor dos Santos, J. P. Araque, R. Cantrill, N. F. Castro, M. C. N. Fiolhais, R. Frederix, R. Gonçalo, R. Martins, R. Santos, J. Silva, A. Onofre, H. Peixoto, and A. Reigoto, Phys. Rev. D **92**, 034021 (2015).

[31] H.-L. Li, P.-C. Lu, Z.-G. Si, and Y. Wang, (2015), arXiv:1508.06416 [hep-ph].

[32] G. Aad *et al.* (ATLAS Collaboration), The European Physical Journal C **75**, 349 (2015), 10.1140/epjc/s10052-015-3543-1.